

**CHARACTERIZATION OF FATIGUE DAMAGE IN A36
STEEL SPECIMENS USING NONLINEAR RAYLEIGH
SURFACE WAVES**

A Thesis
Presented to
The Academic Faculty

by

Simon V. Walker

In Partial Fulfillment
of the Requirements for the Degree
Master of Science in
Engineering Science and Mechanics

School of Civil and Environmental Engineering
Georgia Institute of Technology
December 2011

CHARACTERIZATION OF FATIGUE DAMAGE IN A36
STEEL SPECIMENS USING NONLINEAR RAYLEIGH
SURFACE WAVES

Approved by:

Dr. Laurence J. Jacobs, Advisor
School of Civil and Environmental
Engineering
Georgia Institute of Technology

Dr. Jin-Yeon Kim
School of Civil and Environmental
Engineering
Georgia Institute of Technology

Dr. Jianmin Qu
Department of Civil and Environmental
Engineering
Northwestern University

Date Approved: August 23, 2011

ACKNOWLEDGEMENTS

This thesis would not have been possible without the help and support of many people. First, I would like to thank my advisor Prof. Laurence J. Jacobs for his guidance and support not only throughout the production of this research and thesis but during my whole stay in Atlanta. His financial and organizational commitment also allowed me to present the results of this thesis at the QNDE conference in Burlington, Vermont. Furthermore, I would like to express my gratitude to Dr. Jin-Yeon Kim who was always willing to share his extraordinary knowledge and experience in ultrasonics. He gave me a lot of ideas and advice whenever it was needed. I really enjoyed working with him. I want to thank Prof. Jianmin Qu for serving as a committee member. The experience of Kevin Arne was also very helpful in the beginning of this research. I thank the Mechanical Properties Research Laboratory at the Georgia Institute of Technology for granting me access to their facilities. Special thanks go to Dr. Robert Amaro who was very helpful in every concern about the mechanical testing.

Moreover, I am grateful to Prof. Lothar Gaul for choosing me as a candidate for the ISAP Program. In addition I would like to thank Dr. Helge Sprenger and Dipl.-Ing. Jan Herrmann for their valuable advice and help in organizing the exchange program. I would like to acknowledge the DAAD (German Academic Exchange Service) for providing generous financial support.

I want to thank my fellow students and labmates Katie Matlack, Yu Liu, Charlotte Wheat, Matthias Seher, and Christian Ehrlich for all the assistance, the friendship and the great time we spent together. Finally, I want to express my deepest gratitude to my parents and my family who always supported and encouraged me during this year.

TABLE OF CONTENTS

ACKNOWLEDGEMENTS	iii
LIST OF TABLES	vii
LIST OF FIGURES	viii
LIST OF SYMBOLS	xi
SUMMARY	xii
I INTRODUCTION	1
1.1 Motivation and Objective	1
1.2 Literature Review	2
1.3 Structure of the Thesis	3
II WAVE PROPAGATION IN SOLIDS	4
2.1 Equations of Motion	4
2.2 Linear Wave Propagation	5
2.3 Wave Phenomena	6
2.3.1 Harmonic Waves	7
2.3.2 Reflection at a Stress Free Boundary	8
2.4 Generation of Rayleigh Waves	9
2.5 Characteristics of Rayleigh Waves	10
2.6 Nonlinear Wave Propagation	12
2.6.1 Nonlinearity Parameter β	12
2.6.2 Nonlinear Rayleigh Waves	14
III FATIGUE DAMAGE	17
3.1 Plasticity	17
3.2 Cyclic Deformation	18
3.2.1 Single Crystal	18
3.2.2 Polycrystal	18

IV	SPECIMEN, MECHANICAL TESTING AND ULTRASONIC MEASUREMENT METHOD	20
4.1	Specimens	20
4.2	Mechanical Testing	22
4.2.1	Quasi Static Test	23
4.2.2	Fatigue Test	24
4.3	Ultrasonic Measurement	25
4.3.1	Transducers	26
4.3.2	Wedges	26
4.3.3	Amplifier	27
4.3.4	Oscilloscope	28
4.3.5	Measurement Procedure	28
4.4	Signal Processing	30
4.5	Mechanical Influences on Ultrasonic Measurements	33
4.5.1	Effect of Settling	33
4.5.2	Effect of Misalignment	35
V	EXPERIMENTAL RESULTS	36
5.1	Exploratory Tensile Test	36
5.2	General Results of Ultrasonic Measurement	38
5.2.1	Dependance of Nonlinearity on Propagation Distance	38
5.2.2	Repeatability of Measurement	39
5.3	Influence of Plastic Strain on Acoustic Nonlinearity	41
5.4	Influence of Fatigue Damage on Acoustic Nonlinearity	43
5.4.1	Specimen 1	43
5.4.2	Specimen 2	50
5.4.3	Specimen 3	56
5.4.4	Specimen 4	58
VI	CONCLUSION	62

REFERENCES	64
----------------------	----

LIST OF TABLES

2.1	Relationships between the angles of incident and reflected waves. . . .	8
4.1	Material properties of A36 steel.	20
4.2	Maximum strain values and expected stress for the monotonic tests. .	24
4.3	Maximum stress level for different specimens.	25
4.4	Specifications of the RITEC RAM-5000 system.	27
5.1	Number of fatigue cycles applied on specimen 1.	43
5.2	Number of fatigue cycles applied on specimen 2.	50
5.3	Number of fatigue cycles applied on specimen 3.	56
5.4	Number of fatigue cycles applied on specimen 4.	58

LIST OF FIGURES

2.1	Reflection of P-wave and SV-wave.	8
2.2	Snell's law.	9
2.3	Motion of particles in a Rayleigh surface wave.	11
2.4	Wave propagation in linear and nonlinear materials.	12
4.1	Drawing of the specimen (all dimensions in inches).	21
4.2	Image of a specimen.	21
4.3	Fatigue machine with specimen.	22
4.4	Extensometer fixed on specimen.	23
4.5	Experimental setup for ultrasonic measurement.	25
4.6	Wedge with transducer.	27
4.7	Picture of experimental setup.	29
4.8	Example of the received signal for a undamaged specimen.	31
4.9	Steady-state portion of the received signal.	31
4.10	Example of the Fourier Spectrum.	32
4.11	Normalized second harmonic amplitude.	32
4.12	Change of fundamental amplitude with time.	34
4.13	Change of 2 nd harmonic amplitude with time.	34
4.14	Change of normalized second harmonic amplitude with time.	34
4.15	Effect of misalignment on normalized second harmonic.	35
5.1	Failed specimen after the exploratory test.	36
5.2	Exploratory stress-strain curve.	37
5.3	Normalized second harmonic amplitude versus propagation distance for the undamaged fatigue specimen 1.	38
5.4	Multiple results of normalized second harmonic versus propagation dis- tance.	40
5.5	Stress-strain curves of the monotonic tests.	42
5.6	Normalized acoustic nonlinearity versus total strain.	42

5.7	Stress versus time for the first fatigue test.	44
5.8	Normalized acoustic nonlinearity versus number of fatigue cycles for specimen 1 for $\sigma_{\max} = 1.1 \sigma_{\text{yield}}$, $R=0.05$ and a propagation distance from 7.5 cm to 11.5 cm.	45
5.9	Normalized second harmonic amplitude versus propagation distance for specimen 1 after different numbers of fatigue cycles.	46
5.10	Image of surface damage on fatigue specimen 1.	47
5.11	Amplitude of the fundamental over the propagation distance after 38 cycles.	47
5.12	Amplitude of the second harmonic over the propagation distance after 38 cycles.	47
5.13	Normalized acoustic nonlinearity versus number of fatigue cycles for specimen 1 for a propagation distance from 7.5 cm to 8.5 cm.	48
5.14	Normalized acoustic nonlinearity versus number of fatigue cycles for specimen 1 measured on the backside.	49
5.15	Stress-strain curve for fatigue test 3 on specimen 2.	51
5.16	Stress-strain curve for fatigue test 4 on specimen 2.	51
5.17	Normalized second harmonic amplitude versus propagation distance for the undamaged specimen and after 88 cycles of fatigue.	52
5.18	Normalized second harmonic amplitude versus propagation distance after the first three fatigue tests.	53
5.19	Normalized acoustic nonlinearity and cumulative plastic strain versus number of fatigue cycles for specimen 2 for $\sigma_{\max} = 1.15 \sigma_{\text{yield}}$, $R=0.05$, and a propagation distance from 7.5 cm to 11.5 cm.	54
5.20	Normalized acoustic nonlinearity and cumulative plastic strain versus number of fatigue cycles for specimen 2 for $\sigma_{\max} = 1.1 \sigma_{\text{yield}}$, $R=0.05$ and a propagation distance from 8.5 cm to 10.5 cm.	55
5.21	Normalized acoustic nonlinearity and cumulative plastic strain versus number of fatigue cycles for specimen 3 for $\sigma_{\max} = 1.06 \sigma_{\text{yield}}$, $R=0.05$ and a propagation distance from 7.5 cm to 11.5 cm.	57
5.22	Normalized acoustic nonlinearity and cumulative plastic strain versus number of fatigue cycles for specimen 4 for $\sigma_{\max} = 1.16 \sigma_{\text{yield}}$, $R=0.05$ and a propagation distance from 7.5 cm to 11.5 cm.	59
5.23	Normalized second harmonic amplitude versus propagation distance for specimen 4 after different numbers of fatigue cycles.	60

LIST OF SYMBOLS

Symbol	Description
A, B	amplitudes
A_1	amplitude of the fundamental frequency
A_2	amplitude of the second harmonic
b_i	body forces
c	wave speed
C_{ijkl}	fourth order stiffness tensor
c_L, c_S, c_R	longitudinal, transverse and Rayleigh wave speed
C_1, C_2	constants
\mathbf{d}	unit vector in direction of particle motion
E	young's modulus
E_{ij}	Lagrangian strain tensor
f	frequency
F_{ij}	deformation gradient tensor
k	wavenumber
n_j	normal vector
\mathbf{p}	unit vector in direction of propagation
R	stress Ratio
S	surface
t_i	traction
u_i	displacement
\bar{u}_z	out-of-plane displacement at the surface
V	volume
x	propagation distance
\mathbf{x}	position vector

Symbol	Description
β	nonlinearity parameter
δ_{ij}	Kronecker delta
ϵ_{ij}	strain tensor
ϵ_{\max}	total strain value
λ	wavelength
λ, μ	Lamé constants
ν	Poisson's ratio
ρ	density
σ_{ij}	stress tensor
$\sigma_{\max}, \sigma_{\min}$	maximum and minimum stress during fatigue
σ_{yield}	yield stress
σ_{ult}	ultimate tensile stress
ϕ_R	critical angle for Rayleigh wave excitation
φ, ψ	displacement potentials
ω	angular frequency
∇	Nabla operator

SUMMARY

A36 steel is a commonly used material in civil engineering structures where fatigue damage can lead to catastrophic failure. In this research, nonlinear Rayleigh surface waves are used to characterize damage in A36 steel specimens caused by monotonic tension and low cycle fatigue. Fatigue damage produces the increased acoustic nonlinearity that leads to the generation of measurable higher harmonics in an initially monochromatic Rayleigh wave signal. One specimen is subjected to static tension and four specimens are used for low cycle fatigue tests in the tension-tension mode with a constant stress amplitude. The fatigue tests are interrupted at different numbers of cycles for the nonlinear ultrasonic measurements. Tone burst Rayleigh wave signals are generated and detected using a pair of oil coupled wedge transducers. The amplitudes of the first and second harmonic are measured at varying propagation distances to obtain the nonlinearity parameter for a given damage state. The experimental results show an increase of acoustic nonlinearity in the early stages of fatigue life. Furthermore, a close relationship between plastic deformation and the acoustic nonlinearity is found, which indicates that the acoustic nonlinearity is indeed a measure of microplasticity in this material.

CHAPTER I

INTRODUCTION

1.1 Motivation and Objective

Structural steels like A36 steel are commonly used in the civil infrastructure in structures like bridges. If these structures are repeatedly subjected to high loads, fatigue can lead to catastrophic failure. An example is the incident of the I-35W Mississippi River Bridge in Minneapolis, Minnesota, that killed and injured 158 people, and caused economical damage of more than 10 billion dollars to the U.S. in 2007. More information about this incident can be found in [12]. Civil engineering structures in general tend to be large, complex and unique in shape and are therefore expensive to repair or rebuild. Due to that, a reliable technique is needed that allows the characterization of fatigue damage before failure.

Changes in the material microstructure before crack initiation cannot be reliably measured using linear ultrasonic or other nondestructive evaluation (NDE) techniques. However, the increasing dislocation density due to fatigue causes a nonlinear distortion in an ultrasonic wave. This results in the creation of measurable higher harmonic components in the ultrasonic signals that are transmitted through the fatigue damaged material. This acoustic nonlinearity can be measured using Rayleigh surface waves. Using this wave type has several advantages. The energy of Rayleigh waves is concentrated near the free surface of the material, where fatigue damage is typically initiated. Furthermore, unlike in bulk wave techniques, the wave is generated and detected on the same side of the material. Therefore, access to only one side of the material is required. In addition, Rayleigh waves are able to propagate long distances without significant loss of acoustic energy.

The objective of this research is to experimentally characterize the nonlinear behavior, and thus the damage state in A36 steel undergoing monotonic tension and cyclic fatigue load. A reliable experimental method is used to generate and analyze nonlinear Rayleigh surface waves. The measured acoustic nonlinearity parameters are further related to other damage indicators.

1.2 Literature Review

Ultrasonic measurements are commonly used in nondestructive evaluation. Linear ultrasonic methods include attenuation and velocity measurements. The sensitivity of these techniques however, is limited the detection of large defects. Over the last years, nonlinear ultrasonic techniques have shown their capability of detecting damage in an early stage. Nonlinear ultrasound is able to measure microplasticity. The dependence of the material acoustic nonlinearity parameter on microstructural features for face-centered-cubic metals has been theoretically analyzed by Cantrell et al. [5]. The influence of fatigue-induced dislocation substructures is described in [7]. Furthermore, a different model to quantify the acoustic nonlinearity parameter due to elastic-plastic deformation is developed in [16].

Experimental techniques using different wave types have been developed. Nonlinear longitudinal waves have shown to be useful in characterizing creep damage [25] and have also been used to analyse fatigue damage in aluminium [6] and pearlitic steels [22]. Lamb waves have been applied to characterize the effects of aging and fatigue damage [21]. As mentioned earlier, one characteristic of Rayleigh waves is that the energy is concentrated near the free surface. This makes Rayleigh waves ideal for applications where near-surface effects are important. One way of measuring the signal of a Rayleigh wave that propagates through a material is the use of a laser interferometer system. Blackshire et al. [4] used this technique to assess the local fatigue damage in a titanium sample and Herrmann et al. [13, 14] characterized

damage in a nickel-base superalloy. Barnard et al. [3] used fluid coupled transducers instead of the laser technique for generation and detection of the signal in order to monitor damage accumulation during four-point bending fatigue. Liu et al. [18] showed that wedges made of Plexiglas can be used to launch and detect nonlinear Rayleigh surface waves and used this technique to analyze the effect of shot peening.

1.3 Structure of the Thesis

The outline of this this thesis is as follows. Chapter 2 first provides a brief review of the theory on linear wave propagation and wave phenomena, before Rayleigh surface waves and nonlinear wave propagation are described in greater detail. In Chapter 3 the damage mechanism of fatigue is explained. After that the design of the used specimens is specified in Chapter 4. This chapter also illustrates the mechanical testing methods and explains the experimental setup used for the ultrasonic measurements. Furthermore, the signal processing procedure is described and mechanical influences on the measurement are mentioned. The experimental results of the ultrasonic measurements for the different damage states are presented in Chapter 5. Finally, the results are discussed and conclusions are drawn in Chapter 6.

CHAPTER II

WAVE PROPAGATION IN SOLIDS

This chapter describes the theory of wave propagation in elastic solids. At first the equations of motion are derived. Then, linear wave propagation and wave phenomena are considered. After explaining the characteristics of Rayleigh surface waves, nonlinear wave propagation is described and the acoustic nonlinearity parameter is introduced.

2.1 Equations of Motion

In order to get Cauchy's equation of motion for a body of volume V and surface S , consider the balance of linear momentum which is given by

$$\int_S t_i dS + \int_V \rho b_i dV = \frac{d}{dt} \int_V \rho \dot{u}_i dV \quad (2.1)$$

Here ρ denotes the material mass density, t_i represents the traction, b_i represents body forces, and \dot{u}_i is the time derivative of the displacement u_i , namely, the velocity.

If the Cauchy formula

$$t_i = \sigma_{ij} n_j \quad (2.2)$$

with the stress tensor σ_{ij} and normal vector n_j is substituted into the balance of linear momentum (2.1) and the Gauss' theorem is used to transform the surface integral into a volume integral

$$\int_V (\sigma_{ij,j} + \rho b_i - \rho \ddot{u}_i) dV = 0 \quad (2.3)$$

is obtained. Since this equation has to be true for any volume V the localization argument can be applied. This results in Cauchy's equation of motion

$$\sigma_{ij,j} + \rho b_i = \rho \ddot{u}_i. \quad (2.4)$$

2.2 Linear Wave Propagation

If the propagation of waves is considered, it is more convenient to express the equation of motion (2.4) solely in terms of the displacement instead of the stress (σ_{ij}) and the displacement (u_i). In general, the relationship between stress and strain tensor (ϵ_{kl}) is given using the fourth order stiffness tensor C_{ijkl} by

$$\sigma_{ij} = C_{ijkl}\epsilon_{kl}. \quad (2.5)$$

For an elastically homogeneous isotropic medium the coefficients C_{ijkl} are constants and of the following form [1],

$$C_{ijkl} = \lambda\delta_{ij}\delta_{kl} + \mu(\delta_{ik}\delta_{jl} + \delta_{il}\delta_{jk}) \quad (2.6)$$

where λ and μ denote the Lamé's elastic constants. By plugging (2.6) into (2.5) Hooke's law for a homogeneous, isotropic, and linear elastic medium is obtained,

$$\sigma_{ij} = \lambda\epsilon_{kk}\delta_{ij} + 2\mu\epsilon_{ij}. \quad (2.7)$$

Using the relationship between the strain and the displacement,

$$\epsilon_{ij} = \frac{1}{2}(u_{i,j} + u_{j,i}) \quad (2.8)$$

and substituting (2.7) into the equations of motion (2.4) leads to the Navier's equations of motion

$$\mu u_{i,jj} + (\lambda + \mu)u_{j,ji} = \rho\ddot{u}_i, \quad (2.9)$$

where body forces are neglected. In vector notation (2.9) is given by

$$\nabla^2 \mathbf{u} + (\lambda + \mu)\nabla\nabla\mathbf{u} = \rho\ddot{\mathbf{u}}. \quad (2.10)$$

In order to uncouple these coupled partial differential equations the Helmholtz decomposition

$$\mathbf{u} = \nabla\varphi + \nabla \times \boldsymbol{\psi} \quad (2.11)$$

is introduced. Here, the four functions ϕ , ψ_1 , ψ_2 and ψ_3 are used to represent the three components of \mathbf{u} . Therefor the additional constraint condition

$$\nabla \cdot \boldsymbol{\psi} = 0 \quad (2.12)$$

is necessary to guarantee uniqueness. If the Helmholtz decomposition (2.11) is substituted into Navier's equations of motion (2.10) two uncoupled wave equations in terms of the displacement potentials are obtained,

$$\nabla^2 \varphi = \frac{1}{c_L^2} \ddot{\varphi} \quad \text{and} \quad \nabla^2 \boldsymbol{\psi} = \frac{1}{c_S^2} \ddot{\boldsymbol{\psi}}. \quad (2.13)$$

c_L defines the wave speed of the longitudinal wave (also known as dilatational, irrotational, pressure or P-wave) and c_S represents the wave speed of the vertically and horizontally polarized shear waves (or transverse, rotational, distortional or S-wave). The wave speeds can be expressed by the material properties as

$$c_L = \sqrt{\frac{\lambda + 2\mu}{\rho}} \quad \text{and} \quad c_S = \sqrt{\frac{\mu}{\rho}}. \quad (2.14)$$

Note that $c_L > c_S$ always holds true. The Lamé constants λ and μ are related to the material properties Young's Modulus E and Poisson's ratio ν by

$$\lambda = \frac{E\nu}{(1+\nu)(1-2\nu)} \quad \text{and} \quad \mu = \frac{E}{2(1+\nu)}. \quad (2.15)$$

2.3 Wave Phenomena

In this section the wave phenomena are discussed under the assumption of a plane wave which means a wave with constant properties on a plane perpendicular to its propagation direction, \mathbf{p} . Its mathematical representation is given by

$$\mathbf{u} = \mathbf{d}f(\mathbf{x} \cdot \mathbf{p} - ct). \quad (2.16)$$

Here c is either the longitudinal wave speed c_L or the transverse wave speed c_S , \mathbf{d} is the unit vector defining the direction of particle motion, f is a function that describes

the spatial shape of the wave and \mathbf{x} denotes the position vector. Substitution of (2.16) into (2.10) leads to

$$(\mu - \rho c^2)\mathbf{d} + (\lambda + \mu)(\mathbf{p} \cdot \mathbf{d})\mathbf{p} = 0. \quad (2.17)$$

\mathbf{p} and \mathbf{d} are two different unit vectors, therefore there are only two ways to satisfy (2.17), either $\mathbf{d} = \pm\mathbf{p}$, or $\mathbf{p} \cdot \mathbf{d} = 0$.

1. $\mathbf{d} = \pm\mathbf{p}$ is equivalent to $\mathbf{d} \cdot \mathbf{p} = \pm 1$. Therefore (2.17) yields c_L as given in (2.14).

In this case \mathbf{d} and \mathbf{p} are parallel which means that the motion of the particles is in the direction of propagation. This wave is called longitudinal wave.

2. $\mathbf{p} \cdot \mathbf{d} = 0$ together with (2.17) yields c_S as defined in (2.14). This describes a

transverse wave where the motion of the particles is perpendicular to the direction of propagation. Usually the (x_1x_2) -plane is chosen to contain the vector

\mathbf{p} , motions in the (x_1x_2) -plane are then considered to be vertically polarized (SV-wave), whereas motions normal to the (x_1x_2) -plane are considered to be

horizontally polarized (SH-wave).

2.3.1 Harmonic Waves

In many applications it is useful to consider waves showing harmonic behavior in time and space. A representation of the displacement field of a harmonic wave with amplitude A in the (x_1x_2) -plane is given by

$$\mathbf{u}^{(n)} = A_n \mathbf{d}^{(n)} \exp \left[i k_n (x_1 p_1^{(n)} + x_2 p_2^{(n)} - c_n t) \right]. \quad (2.18)$$

Here n is used to describe the wave type (longitudinal or transverse), k_n and c_n denote the wavenumber and wavespeed respectively, and $\mathbf{d}^{(n)}$ denotes the respective unit vector. The wavenumber k is defined using the angular frequency $\omega = 2\pi f$ as

$$k = \frac{\omega}{c} = \frac{2\pi f}{c} = \frac{2\pi}{\lambda} \quad (2.19)$$

where f is the frequency and λ is the wavelength.

2.3.2 Reflection at a Stress Free Boundary

So far, the propagation of waves in an infinite media has been considered. In the case of a finite medium the effects of reflection and coupling have to be taken into account. At a stress free boundary, i.e. $\sigma_{21} = \sigma_{22} = 0$ an incident P-wave gives rise to a reflected P-wave as well as to a reflected SV-wave. In an analogous manner, an incident SV-wave produces a reflected SV-wave as well as a P-wave. Figure 2.1 shows the two cases.

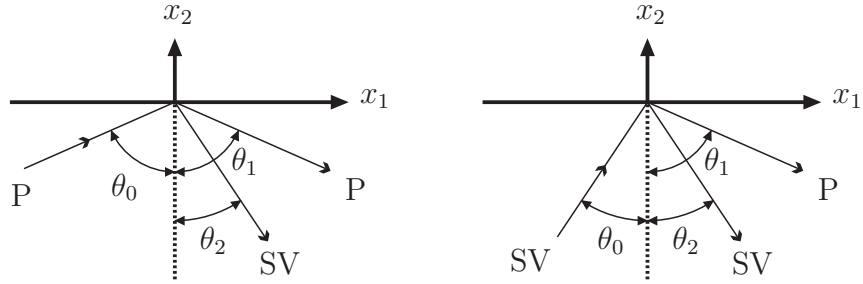


Figure 2.1: Reflection of P-wave and SV-wave.

Using the description of the displacement field given in Equation (2.18) together with the assumption of a constant angular frequency for incident and reflected waves the relationships between the angles of the incident and reflected waves can be obtained. Table 2.1 shows these relationships.

Table 2.1: Relationships between the angles of incident and reflected waves.

Incident θ_0	Reflected P θ_1	Reflected SV θ_2
P	$\theta_1 = \theta_0$	$\sin\theta_2 = (c_S/c_L)\sin\theta_0$
SV	$\sin\theta_1 = (c_L/c_S)\sin\theta_0$	$\theta_2 = \theta_0$

Non-trivial amplitudes A_n occur if the angles of the incident and reflected waves satisfy Snell's law given by

$$k_0 \sin\theta_0 = k_1 \sin\theta_1 = k_2 \sin\theta_2. \quad (2.20)$$

Two special cases have to be taken into account. If the incident wave is normal to

the free surface, i.e. $\theta_0 = 0$ the waves are reflected as themselves. Furthermore, for angles θ_0 greater than the critical angle

$$\theta_{\text{critical}} = \arcsin \frac{c_S}{c_L} \quad (2.21)$$

only a SV-wave is reflected and the P-wave part of the reflection is degenerated into a Rayleigh surface wave. This specific wave type is used in this research to detect damage. In Section 2.5 the details about this wave are presented.

2.4 Generation of Rayleigh Waves

The most commonly used method to generate Rayleigh surface waves is the wedge method. This method is based on the generation of Rayleigh waves by the refraction of longitudinal waves at the interface between two materials. To generate the Rayleigh waves the angle of the longitudinal waves hitting the boundary between the materials has to satisfy the Rayleigh wave excitation condition. Using the velocities c_1 and c_2 Snell's law can be written as

$$c_1 \sin \phi_2 = c_2 \sin \phi_1 \quad (2.22)$$

where ϕ_1 and ϕ_2 are the incident and refraction angles of the longitudinal waves in medium 1 and 2 as depicted in Figure 2.2.

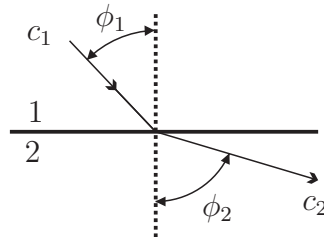


Figure 2.2: Snell's law.

If the incident wave is a longitudinal wave having the velocity $c_1 = c_L$ and in order to receive a surface wave the angle $\phi_2 = 90^\circ$, the critical angle $\phi_1 = \phi_R$ is given by

$$\sin \phi_R = \frac{c_L}{c_R} \quad (2.23)$$

where c_2 is replaced by the Rayleigh wave speed c_R . Note that this relationship holds only when $c_L < c_R$.

2.5 Characteristics of Rayleigh Waves

Rayleigh waves are guided waves that propagate large distances along a free surface. In 1885 Lord Rayleigh first demonstrated that a wave exists which is able to propagate along a stress free surface but its amplitude exponentially decays with depth. Along the free boundary the waves cancel the stresses they produce. A detailed derivation of the mathematical description of Rayleigh waves can be found in Viktorov [26] and Achenbach [1]. In the following, a brief overview is given. In order to derive the equation of the phase velocity of Rayleigh waves the potentials describing the longitudinal and shear wave parts

$$\varphi = C_1 e^{-k_R q z} e^{i k_R (x - c_R t)} \quad (2.24)$$

and

$$\psi = C_2 e^{-k_R h z} e^{i k_R (x - c_R t)} \quad (2.25)$$

are introduced. Here, C_1 and C_2 are arbitrary constants, $q = \sqrt{1 - (\frac{c_R}{c_L})^2}$, $h = \sqrt{1 - (\frac{c_R}{c_S})^2}$ and $c_R = \frac{\omega}{k_R}$ where c_R is the Rayleigh wavenumber. Together with the wave equations (2.13) and after applying the stress free boundary condition, the Rayleigh characteristic equation

$$\left(2 - \frac{c_R^2}{c_S^2}\right)^2 - 4\sqrt{\left(1 - \frac{c_R^2}{c_L^2}\right)\left(1 - \frac{c_R^2}{c_S^2}\right)} = 0 \quad (2.26)$$

is obtained. Since the frequency is not involved in (2.26) the phase velocity of Rayleigh waves does not depend on the frequency, and thus surface waves are nondispersive. Rayleigh waves travel at about 90 % of the shear wave velocity [26]. A good approximation of the Rayleigh wave speed c_R is given in [1] by

$$c_R = \frac{0.862 + 1.14\nu}{1 + \nu} c_S \quad (2.27)$$

where ν donates the Poisson's ratio. The displacement field of a Rayleigh wave is a combination of a longitudinal and a shear displacement which results in an elliptical motion at the surface. The displacements along the x and z axis are phase-shifted by $\pi/2$. As described by Graff [9], the vertical displacement is typically 1.5 times greater than the horizontal component at the surface. For a wave travelling to the right the elliptical partial motion at the surface is counter clockwise. Away from the surface, the amplitude decreases exponentially. In addition, the direction of particle rotation reverses at a depth of about 0.192 times the wavelength. As mentioned earlier the amplitude of the displacement reduces with increasing depth. According to Achenbach's [1] numerical results the relative displacement approaches zero for a distance of more than 1.5 times the wavelength. Figure 2.3 shows the particle motion during the propagation of a Rayleigh surface wave along the positive x -axis.

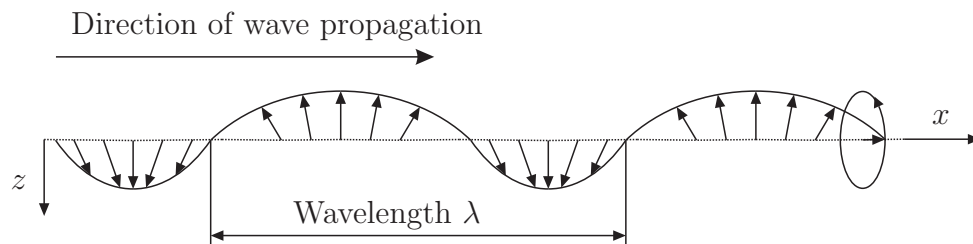


Figure 2.3: Motion of particles in a Rayleigh surface wave.

Rayleigh surface waves are useful for various applications. The fact that most of the energy concentrates near the free surface allows the characterization of the surface layer of a material and the detection of damage and small cracks using ultrasonic techniques. At low frequencies, Rayleigh waves are of particular importance in seismology [9] and can even be used to detect landmines [17]. Furthermore, Rayleigh waves are capable of propagating along smooth curved surfaces and therefore allow the inspection of areas that are difficult to access otherwise [15].

2.6 Nonlinear Wave Propagation

This section deals with the one-dimensional nonlinear wave propagation. In a linear medium only the excited frequency will be detected after the wave propagated through the material. However, in nonlinear materials higher harmonic frequencies will occur, as shown in Figure 2.4. The frequencies of these higher harmonics are integer multiples of the excited fundamental frequency.

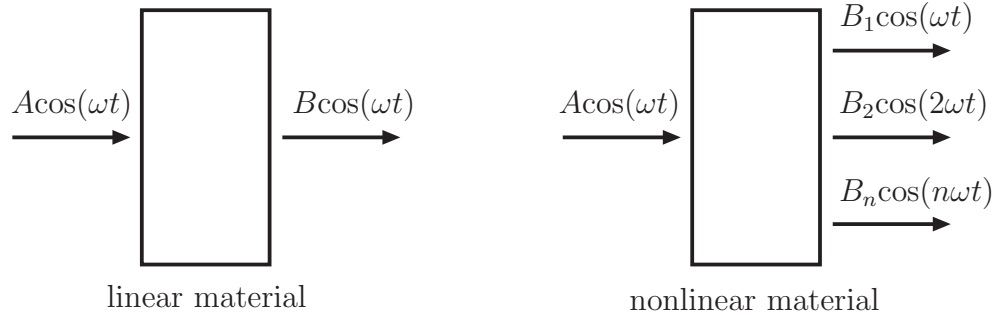


Figure 2.4: Wave propagation in linear and nonlinear materials.

The nonlinearity of a material is caused by inherent lattice anharmonicities, precipitates, and/or vacancies. Furthermore, damage due to plastic deformation including dislocations or microcracks can generate nonlinearity. If an initially sinusoidal stress wave propagates through a nonlinear medium, it distorts and transfers energy from the fundamental to the higher harmonics that appear. The degree of distortion and harmonic generation depends on the amplitude of the fundamental wave [10].

2.6.1 Nonlinearity Parameter β

In this section, an expression for the nonlinearity parameter β is derived. The given derivation follows Hamilton and Blackstock [11]. In nonlinear elasticity the Lagrangian (material) coordinate X is usually used. With the current coordinate of a particle x the displacement u is given as $u = x - X$. The current and material descriptions are related through the deformation gradient tensor by

$$F_{ij} = \frac{\partial x_i}{\partial X_j}. \quad (2.28)$$

The Lagrangian strain tensor is given by

$$E_{ij} = \frac{1}{2} \left(\frac{\partial u_i}{\partial X_j} + \frac{\partial u_j}{\partial X_i} + \frac{\partial u_k}{\partial X_i} \frac{\partial u_k}{\partial X_j} \right). \quad (2.29)$$

The equation of motion can be written in Lagrangian coordinates if the first Piola-Kirchhoff stress tensor (or Lagrangian stress tensor) P_{ij} is used

$$\rho_0 \frac{\partial^2 u_i}{\partial t^2} = P_{ij,j}. \quad (2.30)$$

For small strains the specific strain energy per unit mass W is assumed to have the following expansion

$$\rho_0 W = \frac{1}{2} C_{ijkl} E_{ij} E_{kl} + \frac{1}{6} C_{ijklmn} E_{ij} E_{kl} E_{mn} + \dots, \quad (2.31)$$

where the C_{ijkl} and C_{ijklmn} are the second- and third-order elastic constants respectively. Using the relationship $P_{ij} = \rho_0 \partial W / \partial F_{ij}$ one obtains the expression

$$P_{ij} = C_{ijkl} \frac{\partial u_k}{\partial X_l} + \frac{1}{2} M_{ijklmn} \frac{\partial u_k}{\partial X_l} \frac{\partial u_m}{\partial X_n} + \dots \quad (2.32)$$

where the higher-order coefficients M_{ijklmn} are given by

$$M_{ijklmn} = C_{ijklmn} + C_{ijln} \delta_{km} + C_{jnkl} \delta_{im} + C_{jlmn} \delta_{ik}. \quad (2.33)$$

Combining (2.30) and (2.33) leads to the nonlinear equation of motion

$$\rho_0 \frac{\partial^2 u_i}{\partial t^2} = \frac{\partial^2 u_k}{\partial X_j \partial X_l} \left(C_{ijkl} + M_{ijklmn} \frac{\partial u_m}{\partial X_n} + \dots \right). \quad (2.34)$$

If only the one dimensional case of a longitudinal wave is considered, (2.34) reduces to the displacement based nonlinear wave equation

$$\frac{\partial^2 u}{\partial t^2} = c_l^2 \frac{\partial^2 u}{\partial X^2} \left(1 - \beta \frac{\partial u}{\partial X} \right) \quad (2.35)$$

where the material nonlinearity parameter β is given as

$$\beta = - \left(\frac{3}{2} + \frac{C_{1111}}{2\rho_0 c_l^2} \right). \quad (2.36)$$

In order to be able to determine the nonlinearity parameter using experimental methods, an expression for β in terms of harmonic amplitudes is needed. If the source excitation is assumed to be of the form $u_0 \sin(\omega t - kx)$ a perturbation analysis leads to the following solution to the nonlinear wave equation:

$$\begin{aligned} u &= u_0 \sin(\omega t - kx) + \frac{\beta}{8} \left(\frac{\omega u_0}{c_l} \right)^2 x \sin(2\omega t - 2kx) \\ &= A_1 \sin(\omega t - kx) + A_2 \sin(2\omega t - 2kx) \end{aligned} \quad (2.37)$$

where x is the propagation distance of the wave. Using the amplitudes of the first and second harmonic, A_1 and A_2 , the coefficient of nonlinearity can be expressed by

$$\beta = \frac{8c_L^2 A_2}{\omega^2 x A_1^2}. \quad (2.38)$$

If the wavespeed, frequency and propagation distance is known, the nonlinearity parameter can be determined by measuring the amplitudes of the fundamental wave and second harmonic. However, the given derivation for β is only valid for longitudinal waves. An introduction into the nonlinear wave propagation in Rayleigh waves is given in Section 2.6.2.

2.6.2 Nonlinear Rayleigh Waves

While longitudinal waves are sensitive with respect to the generation of higher harmonics, the acoustic nonlinearity for shear waves vanishes in an isotropic material because of the symmetry of the third order elastic constants. Since Rayleigh waves are the superposition of longitudinal and shear waves with the same trace velocity, it can be assumed that Rayleigh waves show a similar behavior as longitudinal waves concerning nonlinear wave propagation. Therefore, the harmonic ratio $\frac{A_2}{A_1^2}$ should be an indication of the nonlinearity. In the following, the nonlinear parameter β for Rayleigh surface waves is derived based on [14].

Consider again a Rayleigh wave propagating in the positive x direction on the surface of a halfspace, where the z direction points into the material. The displacement

potentials already given in (2.24) and (2.25) can also be written as

$$\varphi = -i \frac{B_1}{k_R} e^{-pz} e^{i(k_R x - \omega t)}, \quad (2.39)$$

$$\psi = -i \frac{D_1}{k_R} e^{-sz} e^{i(k_R x - \omega t)}, \quad (2.40)$$

where $p^2 = k_R^2 - k_L^2$ and $s^2 = k_R^2 - k_S^2$; and the subscripts R, L and S for the wavenumbers represent Rayleigh, longitudinal and shear waves respectively. If again the stress free boundary conditions on the surface are applied, a relationship between the constants B_1 and D_1 can be obtained,

$$B_1 = -i \frac{2k_R p}{k_R^2 + s^2} D_1. \quad (2.41)$$

The displacement of the Rayleigh wave can be decomposed into a longitudinal and and shear component,

$$u_x = B_1 \left(e^{-pz} - \frac{2ps}{k_R^2 + s^2} e^{-sz} \right) e^{i(k_R x - \omega t)}, \quad (2.42)$$

$$u_z = iB_1 \frac{p}{k_R} \left(e^{-pz} - \frac{2k_R^2}{k_R^2 + s^2} e^{-sz} \right) e^{i(k_R x - \omega t)}. \quad (2.43)$$

According to [27] the second order harmonic Rayleigh wave in the far field of a medium having a weak quadratic nonlinearity is given by

$$u_x \approx B_2 \left(e^{-2pz} - \frac{2ps}{k_R^2 + s^2} e^{-2sz} \right) e^{i2(k_R x - \omega t)}, \quad (2.44)$$

$$u_z \approx iB_2 \frac{p}{k_R} \left(e^{-2pz} - \frac{2k_R^2}{k_R^2 + s^2} e^{-2sz} \right) e^{i2(k_R x - \omega t)}. \quad (2.45)$$

As described above, only the longitudinal wave contribution leads to the generation of higher harmonics in Rayleigh waves. This allows to relate the amplitudes of the fundamental and second harmonic of the displacement in x direction in a similar fashion as in in bulk longitudinal waves using the acoustic nonlinearity parameter β ,

$$B_2 = \frac{\beta k_L^2 x B_1^2}{8}. \quad (2.46)$$

In this research the wedge method described in Chapter 4 is used to detect the wave. Since fluid is used as a couplant only the out-of-plane motion is measured. The normal

components of the particle displacements u_z on the surface can be related by using (2.43), (2.45) and (2.46) and forming the ratio of the second harmonic amplitude to the fundamental amplitude

$$\frac{\bar{u}_z(2\omega)}{\bar{u}_z^2(\omega)} = \frac{\beta k_L^2 x}{8i(p/k_R)[1 - 2k_R^2/(k_R^2 + s^2)]}, \quad (2.47)$$

where $\bar{u}_z(\omega) = u_z(\omega, x, z = 0)$. Rearranging leads to the nonlinearity parameter in terms of the measured out-of-plane displacement components

$$\beta = \frac{\bar{u}_z(2\omega)}{\bar{u}_z^2(\omega)} \frac{8ip}{xk_L^2 k_R} \left(1 - \frac{2k_R^2}{k_R^2 + s^2} \right). \quad (2.48)$$

Note that Shui and Solodov [23] obtained the same result from a perturbation analysis. The shear wave component by itself does not produce nonlinearity. However, the second term in the bracket in (2.48) describes the contribution of the shear wave component interacting with the longitudinal wave component.

CHAPTER III

FATIGUE DAMAGE

Mechanical fatigue occurs when a material is subjected to fluctuating externally applied stresses or strains. Suresh [24] classifies the progression of fatigue damage into five stages:

1. Microstructural changes causing nucleation of permanent damage
2. Creation of microscopic cracks
3. Formation of 'dominant' cracks by growth and coalescence of microscopic flaws
4. Stable propagation of the dominant macrocrack
5. Structural instability or complete fracture

This research focuses on the characterization of the fatigue damage before crack initiation, i.e. in the stage 1. Therefore, substructural and microstructural changes of the material have to be considered.

3.1 Plasticity

Increasing the load on a ductile material above the elastic limit results in permanent plastic deformation. Assuming the material to be incompressible during the plastic deformation the condition $\epsilon_{ii}^p = 0$ is obtained for the plastic strains ϵ_{ij}^p [24]. Plastic deformation is therefore based on shear strain. This inelastic shear strain is dominantly the result of the movement of dislocations. Unlike in elastic deformation, which is based on the stretching of chemical bonds, atoms change their neighbors in plastic deformation and return to a stable configuration. The dislocations typically travel

along slip planes. On these planes, the atoms are closely-packed which allows them to move easier than in other directions. Often, the plastic deformation in a material concentrates in slip bands, where the slip planes of multiple dislocations accumulate. This results in the formation of regions of high plastic shear deformation that are separated by regions of low shear [8].

3.2 Cyclic Deformation

Getting conclusive results of cyclic deformation mechanisms in commercial alloys is difficult. More information is available about deformation mechanisms in fatigue of high purity materials, especially single crystals of face-centered cubic (FCC) metals.

3.2.1 Single Crystal

If a FCC single crystal, under fully reversed loading is considered, the first point that should be noted is that rapid hardening occurs within the initial few cycles. This hardening corresponds to the accumulation of primary dislocations. If more cycles are applied, a quasi-steady state of deformation (saturation) is reached [24], [19]. It has been shown that basically the entire deformation is carried by persistent slip bands (PSB). In a PSB thousands of single slip planes form a flat lamellar structure which in a single crystal spans the whole cross section of the crystal sample. According to Suresh [24] the PSB is divided into channels by dislocation ladders or walls. These walls are formed by edge dislocations and the deformation in the channels in-between the walls is due to the glide of screw dislocations. PSBs are much softer than the surrounding matrix. The matrix contains vein-like structures that are made up of arrays of edge dislocations.

3.2.2 Polycrystal

Structural steels are composed of an aggregate of small crystal grains. If such a material undergoes cyclic loading, slip bands are first developed in grains having an

unfavorable orientation relative to the applied stress. More of these regions with intense deformation are formed as more cycles are applied. With increasing number of cycles the rate of formation slows down and the number of slip bands approaches a saturation level. Therefore, the present slip bands become more emphasized and some of them develop into cracks within grains. These cracks spread out and join with other cracks thereby forming a large crack which propagates until the failure of the material [8].

CHAPTER IV

SPECIMEN, MECHANICAL TESTING AND ULTRASONIC MEASUREMENT METHOD

In this research Rayleigh surface waves are used to determine the acoustic nonlinearity of A36 steel specimens for different damage states. This chapter describes the specimens and the methods used for mechanical testing and ultrasonic measurements. At first, the design of the specimen is explained. Section 4.2 describes the mechanical testing procedure. Then, the experimental setup and the procedure of the ultrasonic measurements is discussed in Section 4.3. Finally, the signal processing and some mechanical influences on the ultrasonic measurements are described.

4.1 Specimens

The specimens used in this research are made of A36 steel. A36 is chosen because it is a commonly used material for bridge structures in the United States and Europe. The testing method for the A36 standard is established by the American Society for Testing and Materials, ASTM International. Table 4.1 shows the material properties of this steel. In order to characterize the material, exploratory quasi static tensile tests are performed on two specimens without performing ultrasonic tests. Therefore dogbone shaped specimens are machined from the same plate that is used for

Table 4.1: Material properties of A36 steel.

Density	0.28 lbm/in ³ (7.8 g/cm ³)
Minimum yield strength	36,000 psi (250 MPa)
Ultimate tensile strength	58,000-80,000 psi (400-550 MPa)
Young's modulus	29*10 ⁶ psi (200 GPa)

the specimens described later. The gauge section of these specimens have a width of 0.5 in, a thickness of 0.25 in and a length of 2.5 in. The measured stress-strain relationship for this material can be found in Section 5.1.

Since Rayleigh waves are generated by a wedge transducer in this research, a flat, smooth surface on the specimens is essentially needed. The specimens used for the ultrasonic measurements are cut out of a flat plate of thickness 0.25 in. At first, the specimens are designed according to ASTM E8 (Standard Test Methods for Tension Testing of Metallic Materials). However, in order to achieve the desired stress level with the available fatigue machine, the width of the gauge section has to be reduced. Figure 4.1 shows the dimensions of the specimens. The specimens are cut out of a steel

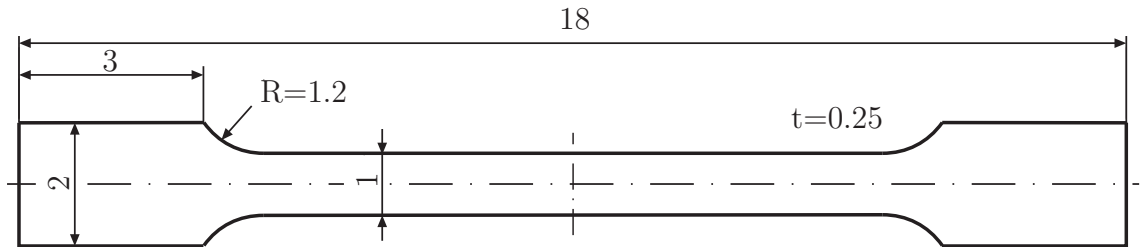


Figure 4.1: Drawing of the specimen (all dimensions in inches).

plate using a water jet cut. The specimens for the fatigue tests are then machined using milling in order to achieve a smooth surface at the edges of the specimens. Finally the top and bottom surfaces of all the specimens are carefully prepared with a surface grinder. This is a very time consuming process, but it is necessary since Rayleigh waves are very sensitiv to the surface conditions, in particular the surface roughness. A picture of a specimen is given in Figure 4.2.



Figure 4.2: Image of a specimen.

4.2 Mechanical Testing

The specimens described in Section 4.1 are subjected to different amounts of tensile loading. For the monotonic and fatigue tests, the same fatigue machine is used. A 20 kip SATEC Uniframe servo hydraulic test frame with a maximum force capacity of 20,000 lbf. Figure 4.3 shows the machine with one of the specimens set up. An extensometer is used to measure the strain in the center part of the specimen. The extensometer attached to the specimen is shown in Figure 4.4. Note that the extensometer doesn't measure the strain of the whole gauge section of the specimen, but the strain in the area where the receiving transducer is scanned. Before each test the machine is warmed up for several minutes by cycling with an amplitude of 0.25 in and a frequency of 1 Hz. Besides the strain, the displacement of the grip and the force is recorded during each measurement as a function of time.

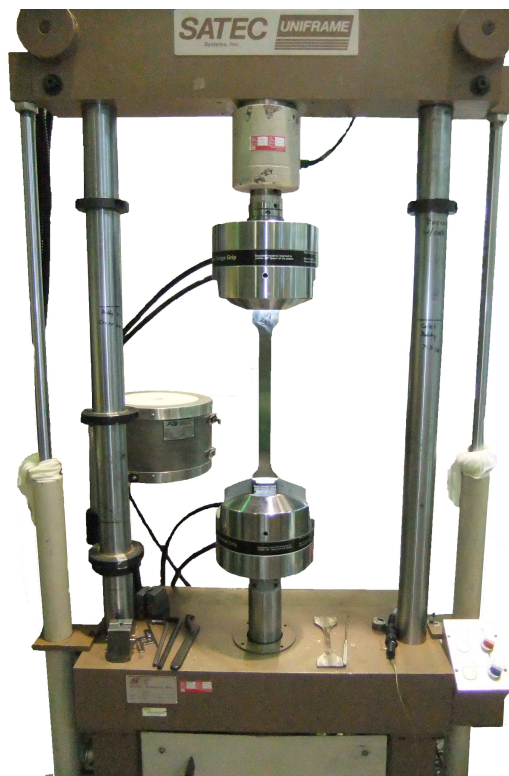


Figure 4.3: Fatigue machine with specimen.

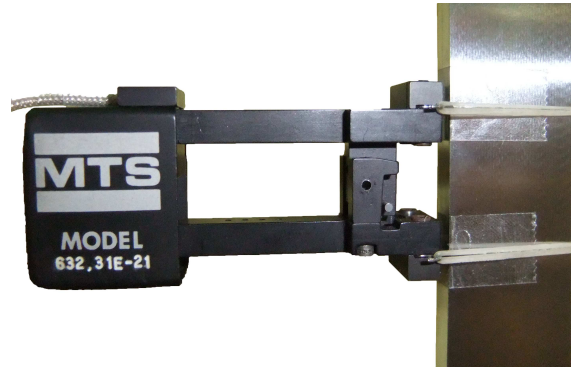


Figure 4.4: Extensometer fixed on specimen.

4.2.1 Quasi Static Test

Before the specimens for the ultrasonic test are considered, exploratory mechanical tests are performed. The purpose of these tests is to get an actual stress-strain curve of the material which allows for choosing the right parameters for the following tests. The uniaxial exploratory tests are performed using a constant rate of head separation (displacement control) of 0.01 in/s. This results in a strain rate of approximately 0.0035 in/in/s.

After performing the exploratory tests, the first specimen used for ultrasonic tests is subjected to monotonic tensile load. The specimen is loaded until a certain strain value is achieved and then immediately unloaded. After that, the specimen is removed from the testing machine and nonlinear ultrasonic measurements are taken as described in Section 4.3. Then, the specimen is mounted in the machine again. The alignment of the specimen with respect to the grips is critical to ensure the consistent loading conditions as before. Now, the strain in the specimen is further increased and the ultrasonic measurement is repeated. This procedure is repeated five times. The total strain values (ϵ_{\max}) and the expected stresses for the five tests are given in Table 4.2. The values of the stresses are obtained from the measured stress-strain curve.

Table 4.2: Maximum strain values and expected stress for the monotonic tests.

Test	ϵ_{\max}	expected stress at ϵ_{\max}
1	$1.2 * 10^{-2}$	55.2 ksi
2	$2.4 * 10^{-2}$	60.8 ksi
3	$3.6 * 10^{-2}$	64.6 ksi
4	$4.8 * 10^{-2}$	67.0 ksi
5	$6.0 * 10^{-2}$	68.4 ksi

The tests are performed under the same conditions as in the exploratory tests. Therefore, displacement control and a rate of 0.01 in/s is used. In order to prevent slip between the grips and the specimen, the maximum available grip pressure of 3000 psi is applied.

4.2.2 Fatigue Test

After the monotonic test on one specimen, four specimens are used for fatigue tests. The procedure is similar to the one for the monotonic tension test. A specimen is mounted on the fatigue machine and after a certain number of fatigue cycles, the test is interrupted. The specimen is unloaded and ultrasonic measurements are taken. After that the specimen is fixed in the machine again and undergoes more cycles of fatigue.

The specimens are designed for the use of the wedge method to generate and detect Rayleigh surface waves. For this reason, the specimens are wide but relatively thin. This design does not allow a compressive load, because bending would occur. The fatigue tests are therefore performed in the tension-tension mode. The stress ratio R between minimum and maximum stress for all tests is chosen as

$$R = \frac{\sigma_{min}}{\sigma_{max}} = 0.05.$$

This ensures that the specimen never undergoes a compressive load. Different maximum stress levels are used for the different specimens. The ratios of maximum stress to yield stress, $\frac{\sigma_{max}}{\sigma_{yield}}$ for the four specimens can be found in Table 4.3.

Table 4.3: Maximum stress level for different specimens.

Specimen	$\sigma_{max}/\sigma_{yield}$
1	1.1
2	1.15
3	1.06
4	1.17

4.3 Ultrasonic Measurement

Rayleigh surface waves can be generated using different techniques. In this work, the wedge-method is used to excite and detect Rayleigh surface waves. The ultrasonic transducers are fixed on wedges. The transmitter produces a sinusoidal toneburst signal of the fundamental frequency. After the waves propagated a certain distance through the material, the receiver detects a signal consisting of the fundamental frequency as well as a second harmonic portion generated by nonlinear distortion in the material. Figure 4.5 shows the experimental setup for the ultrasonic measurement. A high power amplifier (Ritec RAM 5000) is used to generate the high amplitude input

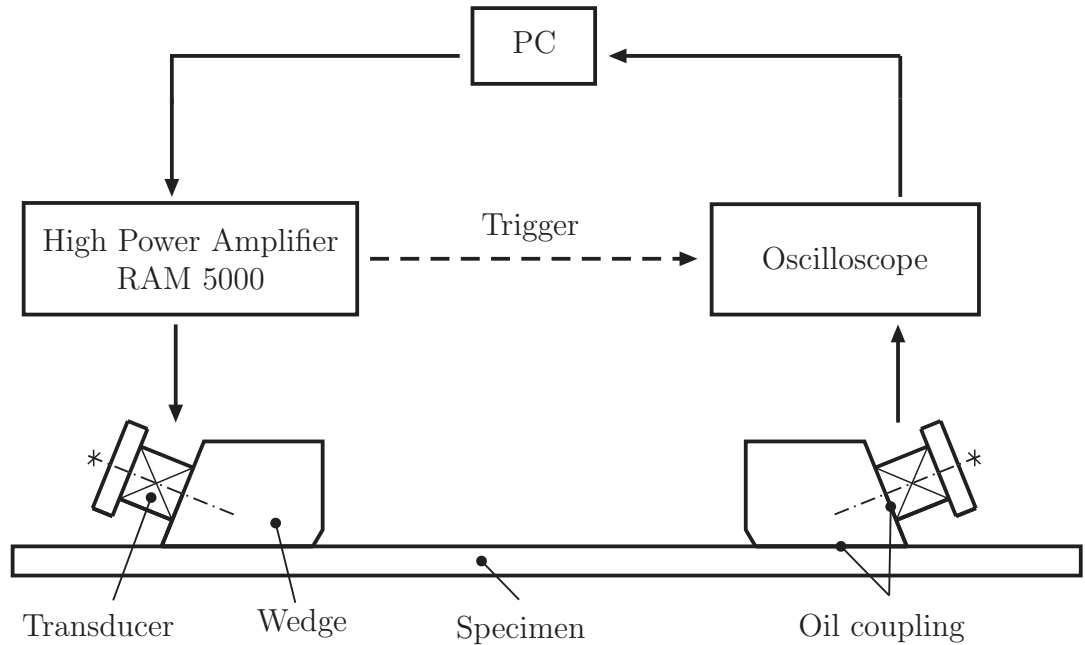


Figure 4.5: Experimental setup for ultrasonic measurement.

signal. Between the transducers and the wedges and in between the wedges and the specimen light lubrication oil is used as couplant. The signals received by the second transducer are recorded by a Tektronix oscilloscope, and then finally are saved on a computer.

4.3.1 Transducers

In these experiments commercial piezoelectric longitudinal wave transducers built by Olympus are used.

- Transmitter: Panametrics X1055, 2.25 MHz, 0.5"
- Receiver: Panametrics X1056, 5 MHz, 0.5"

Both the transducers have a diameter of 0.5 inch. The center frequency of the receiving transducer is chosen as twice the center frequency of the transmitter in order to get a higher sensitivity at the second harmonic. However, the 5 MHz transducer is as well responsive at lower frequencies and is therefore also able to reliably detect the fundamental wave. The transducers are not completely linear, but since the propagation distance of the wave is varied, nonlinear effects of the transducers can be neglected. The transmitting transducer is driven by the high power amplifier described in Section 4.3.3. The high powers that are available can severely damage piezoelectric transducers.

4.3.2 Wedges

The described transducers generate longitudinal waves. To create Rayleigh surface waves, a wedge is needed. The wedges are designed in such a way that the longitudinal wave created by the transducer hits the boundary between wedge and specimen under the Rayleigh critical angle. The expression for this angle is given by Equation (2.23) in Section 2.4. Figure 4.6 shows the acrylic wedge with the mounted transducer. For transmission and detection the same wedges are used.

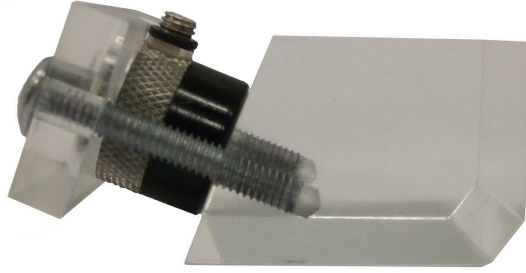


Figure 4.6: Wedge with transducer.

4.3.3 Amplifier

To generate high amplitude ultrasonic signals, a RITEC RAM-5000 MARK IV system is used. This instrument contains a high power gated RF amplifier, an internal trigger generator as well as a cycle counter which allows to determine the width of the produced tone burst. Some specifications of the RITEC RAM-5000 are given in Table 4.4. The high power of this amplifier is very useful in nonlinear ultrasonic measurements. The amplitude of the second harmonic frequency is proportional to the square of the amplitude of the fundamental. A high input power therefore results in much larger amplitudes of the second harmonic compared to low input powers. This allows an efficient detection of the second harmonic within the fundamental wave and the noise. Furthermore, the RITEC RAM-5000 system has the advantage of having a small inherent nonlinearity and creating a clean single frequency output. This ensures that the measured nonlinearity is due to material nonlinearity rather than the nonlinearity of the experimental instrumentation.

Table 4.4: Specifications of the RITEC RAM-5000 system.

Frequency Range for Synthesizer	50 kHz to 22 MHz
Nominal Frequency Range for Gated Amplifier	250 kHz to 17.5 MHz
On/Off Ratio of Gated Amplifier	>140 dB
Typical Gated Amplifier RMS Output Power	1.5 kW between 0.25 and 7 MHz

The same type of input signal is used for all the measurements. The RITEC system creates a sinusoidal tone burst signal. A frequency of 2.1 MHz is chosen since it results in the highest amplitudes with the given set of transducers. The wavelength of the Rayleigh surface wave can be calculated using

$$\lambda = \frac{c_R}{f}. \quad (4.1)$$

With a Rayleigh wave speed of approximately 2900 m/s the wavelength turns out to be 1.38 mm. Therefore, the thickness of the specimens is about 4.6 times higher than the wavelength at the fundamental frequency. This means that almost no displacement occurs at the opposite surface of the specimen. Thus, no reflections from the other side have an influence on the propagating wave and the generated wave truly is a Rayleigh wave instead of a Lamb wave.

The length of the input signal is 35 cycles for sufficient energy and to achieve a large steady state portion so that transient and ringing effects can be neglected. Using an output level of 90 % of the maximum available output level results in a large amplitude of the signal. Furthermore, it has been shown that the amplifier itself has a higher nonlinearity for low output levels. By working at high output levels these nonlinear effects can be reduced.

4.3.4 Oscilloscope

For the signal acquisition the Tektronix TDS 420 Oscilloscope is used. The sampling rate is 100 MS/s and the average of 500 signals is taken in order to increase the signal to noise ratio.

4.3.5 Measurement Procedure

The procedure of the ultrasonic measurement is the same for all measurements that are taken. At first, the specimen is fixed on a stand and carefully aligned to a ruler. The ruler serves as an edge guide to align the wedges to the specimen and is also

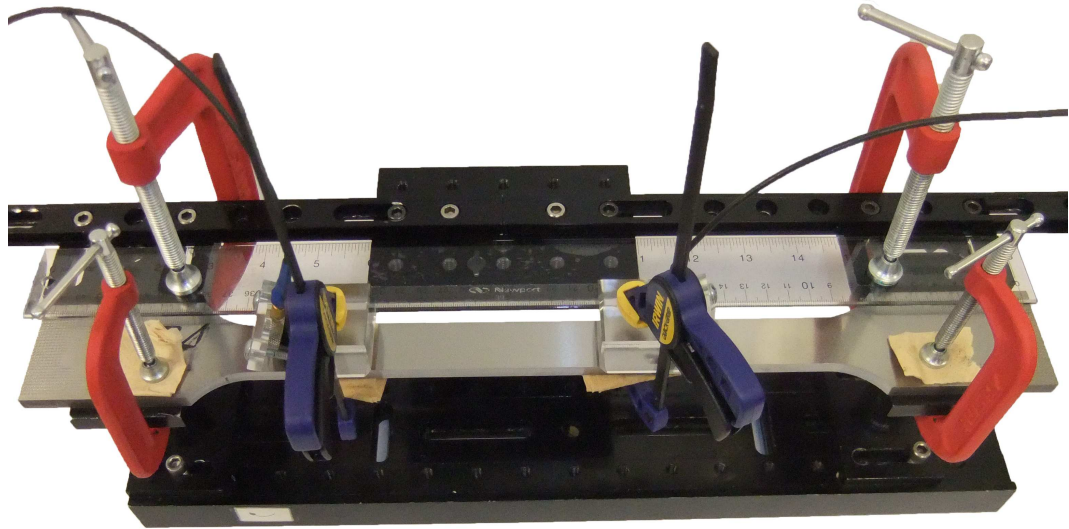


Figure 4.7: Picture of experimental setup.

used to determine the propagation distance between transmitter and receiver. The influence of misalignment can be found in Section 4.5. Before each measurement the transducers are coupled to the wedges. One drop of lubrication oil is used as couplant. The screws in the wedge are fixed with approximately the same force each time. The next step is to fix the transmitting wedge setup on the specimen using oil as couplant and a clamp to hold the wedge in place. Before the measurement is started the RITEC is turned on to warm up and the setup is given 30 minutes to settle. This is needed because it was found that the amplitude of the received signal increases shortly after setting up the equipment. The transmitter will not be moved during one set of measurements. Now, the receiving wedge setup is fixed on the specimen the same way as the transmitter. However, since the propagation distance will be varied, it is not practical to wait 30 minutes each time after setting up the receiver. Because the measurement is always started right after setting up the receiver, the influence of the settling can be neglected. Figure 4.7 shows a picture of the specimen fixed on the stand and the wedges clamped to the specimen. Before the measurement is started, the excess oil on the surface of the specimen, especially around the wedges has to be

cleaned up carefully. This plays an important role in getting repeatable results. Now, the oscilloscope is used to detect the signal. Averaging over 500 signals results in an increased signal to noise ratio. The measured signal is then saved on the computer in an Excel file for further processing. After saving the data for a specific propagation distance, the receiving wedge setup is removed and the oil on the specimen and the wedge is cleaned up. Using one drop of oil again, the wedge is then placed on the next measurement point. These steps are repeated for every propagation distance.

In order to ensure the repeatability of the technique and to eliminate mistakes due to incorrect handling, the complete procedure described above is repeated at least three times for every specimen in each damage state.

4.4 Signal Processing

Figure 4.8 shows the received signal as it is recorded by the oscilloscope for an undamaged specimen. For the further analysis only the steady state portion of the signal is used. Therefore, the first seven cycles at the beginning which contain the transient part and the last few cycles showing a ringing effect are neglected. In Figure 4.9 the steady-state portion of the signal can be seen. A Hann-window is applied before the Fast Fourier Transform (FFT) is performed. The Hann window greatly reduces the amplitude of the side lobes but has the disadvantage of widening the main lobe [20]. Figure 4.10 shows the Fourier spectrum of the signal given in Figure 4.9. Note that the scale of the vertical axis varies for the fundamental and second harmonic. The amplitudes of the fundamental and second harmonic are called A_1 and A_2 respectively. If the described procedure is repeated for the signals received at all different propagation distances, a plot showing the second harmonic amplitude normalized by the square of the fundamental amplitude as a function of propagation distance can be obtained (see Figure 4.11). According to Equation 2.48 the nonlinearity parameter β is proportional to $\bar{u}_z(2\omega)/\bar{u}_z^2(\omega)$ where $\bar{u}_z(\omega)$ and $\bar{u}_z(2\omega)$ are the out-of-plane

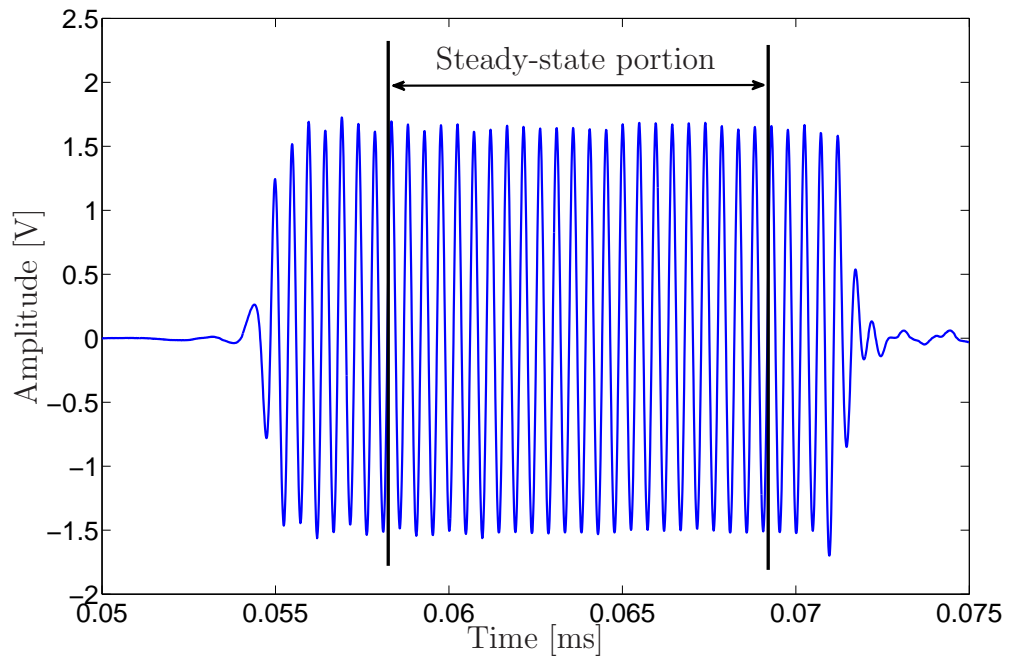


Figure 4.8: Example of the received signal for a undamaged specimen.

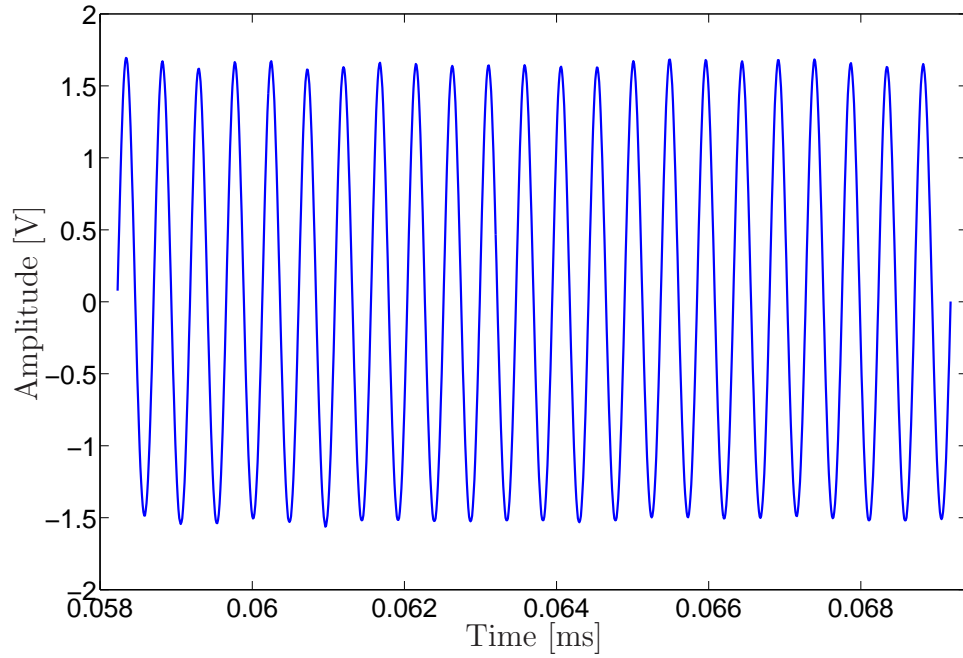


Figure 4.9: Steady-state portion of the received signal.

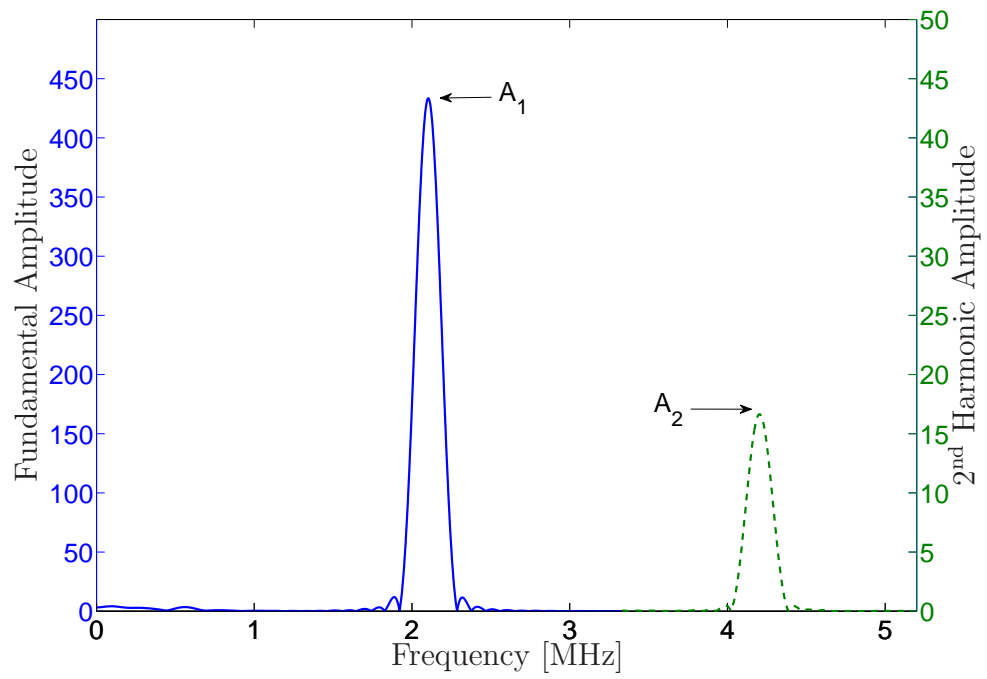


Figure 4.10: Example of the Fourier Spectrum.

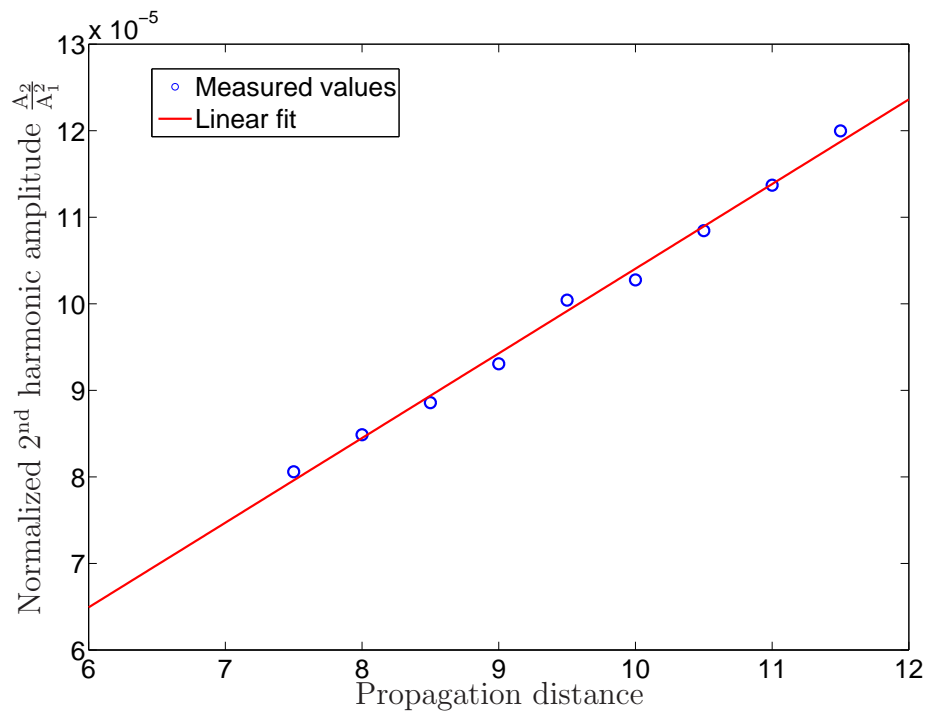


Figure 4.11: Normalized second harmonic amplitude.

displacement components at the fundamental and second harmonic frequency. The amplitudes A_1 and A_2 are proportional to these displacement components. This leads to the proportionality between $\frac{A_2}{A_1}$ and β . Finally, according to Equation (2.47) the slope of the linear fit in Figure 4.11 is proportional to the nonlinearity parameter β . In this research, the slopes of these curves at different damage states of the specimen are therefore compared.

4.5 Mechanical Influences on Ultrasonic Measurements

In order to achieve precise and consistent measurement results, every detail in the procedure is important. In this section the change of the amplitude of the signal with time and the effect of misalignment of the wedges is examined.

4.5.1 Effect of Settling

As mentioned above, the amplitudes of the first and second harmonic change with time after setting up the wedges on the specimen. The influence of settling can be tested by setting up the transmitter and receiver and taking measurements progressively at different times. Neither transmitter, nor receiver are removed in between these measurements. It is important that the RITEC system is given time to warm up before these measurements are taken, since it has been found that the warm up process also has an influence on the signal. Figures 4.12 and 4.13 show that the amplitudes of the fundamental and second harmonic increase with time. Only after 30 to 40 minutes, the amplitudes become more stable. A_1 increases by almost 9% and A_2 even by 17%. The behavior of the normalized second harmonic $\frac{A_2}{A_1}$ with time can be seen in Figure 4.14. The plot shows a decrease in the beginning and almost no change after 40 minutes. The variation between the maximum and minimum values however is only 1.3%. These results show that waiting for 30 minutes after setting up the transmitting wedge is reasonable and ensures that the effects of settling have no noticeable influence on the results.

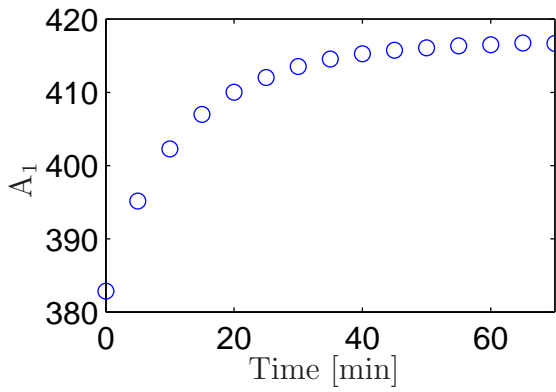


Figure 4.12: Change of fundamental amplitude with time.

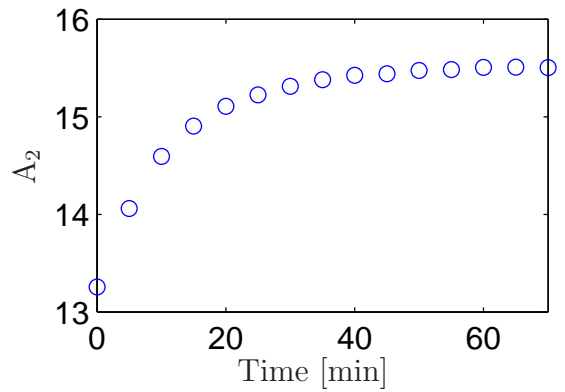


Figure 4.13: Change of 2nd harmonic amplitude with time.

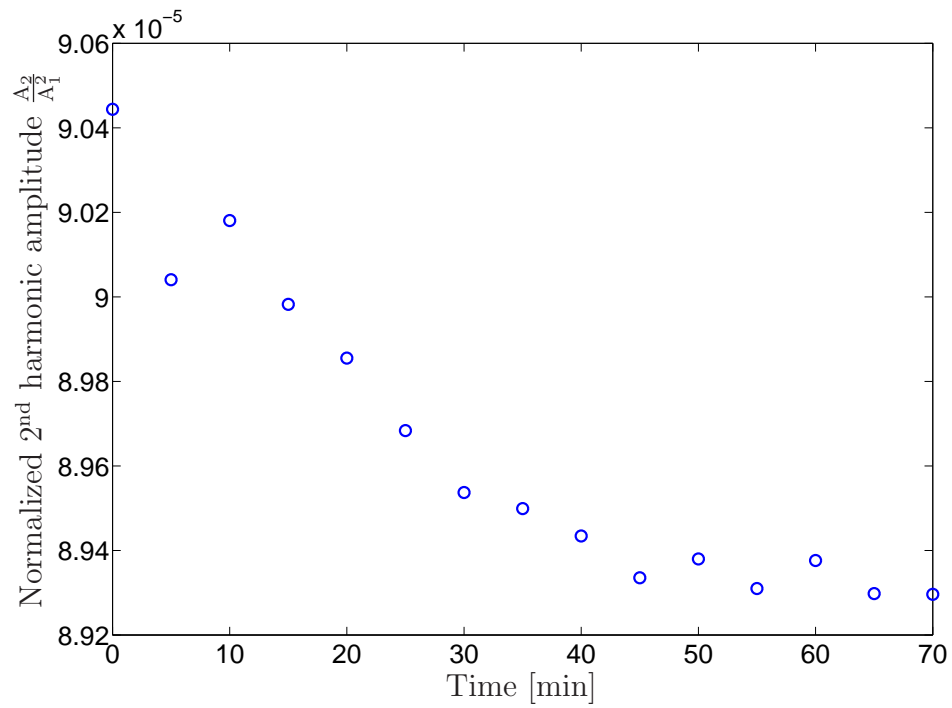


Figure 4.14: Change of normalized second harmonic amplitude with time.

4.5.2 Effect of Misalignment

Especially because the width of the wedge is greater than the width of the specimen, achieving a good alignment of the wedges to the specimen is crucial. Misalignment may lead to a large amount of edge reflections which have an influence on the measured results. To visualize this effect, a measurement on an undamaged specimen is taken where the ruler serving as a guide for the wedges is misaligned by 5° . Figure 4.15 shows the average and the standard deviation of five measurements taken well aligned and the data of the misaligned measurement. The graph shows that the values especially for large propagation distances vary significantly. The slope of the linear fit of the misaligned measurement is much smaller than the one of the reference measurements.

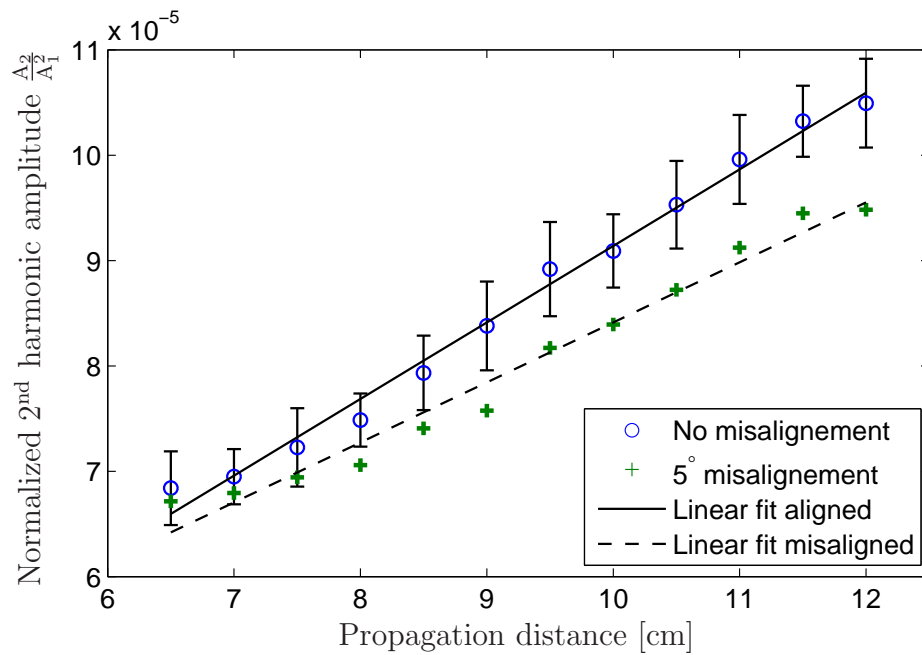


Figure 4.15: Effect of misalignment on normalized second harmonic.

CHAPTER V

EXPERIMENTAL RESULTS

In this chapter the experimental results are presented. First the mechanical properties of the A36 material used are determined by a quasi static tension test. In Section 5.2 the results of ultrasonic measurements are discussed with respect to the used propagation distance and the repeatability of the measurement. Then the influence of plastic deformation on the acoustic nonlinearity is analyzed and finally fatigue damage in A36 steel is characterized. The results for four specimens undergoing cyclic loading are presented separately.

5.1 Exploratory Tensile Test

Before the monotonic load test, exploratory tests are performed on two specimens. One of the failed specimen is shown in Figure 5.1. The typical behavior of necking and a ductile fracture is visible. Figure 5.2 shows the measured stress-strain relationship for this specimen. The second specimen shows the same behavior. The yield stress is found to be $\sigma_{\text{yield}} = 54$ ksi and the ultimate tensile strength is $\sigma_{\text{ult}} = 70$ ksi. The measured yield strength is significantly higher than the nominal minimum yield strength required for A36 steel of 36 ksi. However, studies by the Structural Shape Producers



Figure 5.1: Failed specimen after the exploratory test.

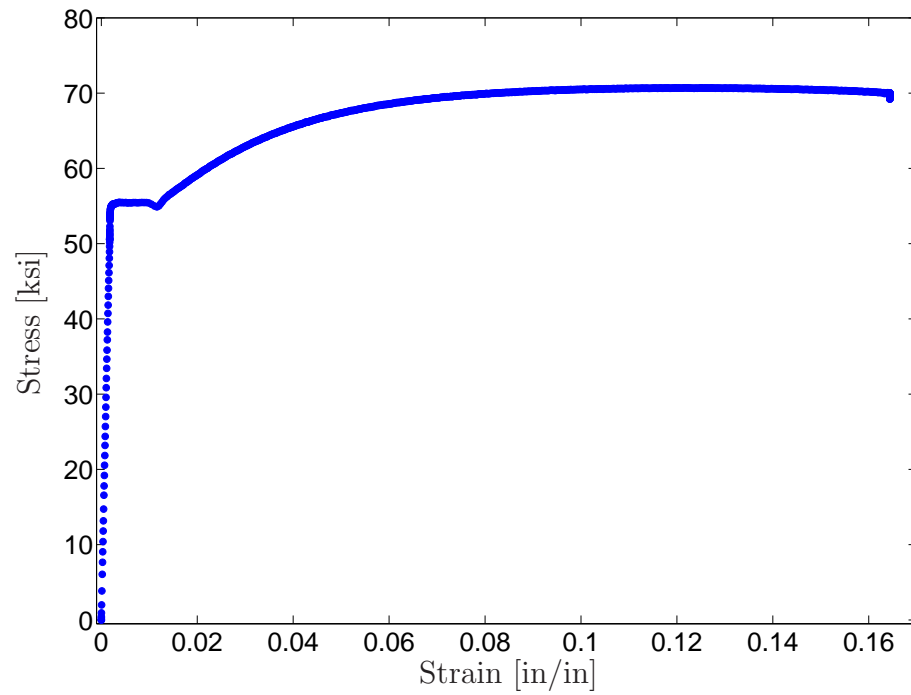


Figure 5.2: Exploratory stress-strain curve.

Council have shown that the actual yield strength of A36 steel often exceeds 50 ksi. The obtained results are later used to determine the load levels for the fatigue tests.

5.2 General Results of Ultrasonic Measurement

5.2.1 Dependence of Nonlinearity on Propagation Distance

In this research the nonlinearity of the material is quantified by taking ultrasonic measurements for increasing propagation distances. As a first step, the range of the propagation distance has to be determined. Figure 5.3 shows the normalized second harmonic amplitude versus the propagation distance for an undamaged specimen. This specimen is later used for fatigue tests (see Section 5.4.1). The ultrasonic measurements are taken twice which results in the error bars as shown in Figure 5.3. According to the theory described in Section 2.6.2, the relationship between the normalized second harmonic amplitude $\frac{A_2}{A_1^2}$ and the propagation distance is linear. In Figure 5.3 this is not the case for the whole range of the propagation distance. For a small propagation distance, the near field of the transducer has an influence on

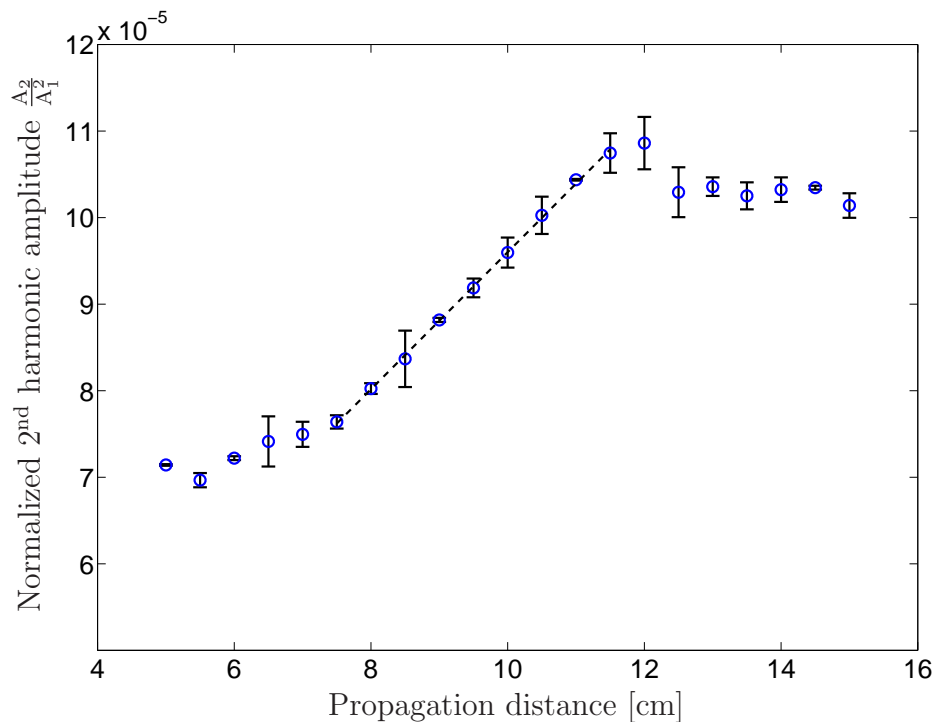


Figure 5.3: Normalized second harmonic amplitude versus propagation distance for the undamaged fatigue specimen 1.

the results. On the other hand, for large propagation distances above 12 cm, the geometric spreading and the attenuation due to the surface roughness as well as the material absorption lead to a decrease in the relative nonlinearity parameter. However, in between 7.5 cm and 11.5 cm the plot shows a very linear trend. The same behavior is observed for different specimens. Therefore, this range of propagation distances is used to determine the nonlinearity parameter.

5.2.2 Repeatability of Measurement

In order to perform a monotonic tension or fatigue test, the specimen has to be removed from the fixture used for the ultrasonic tests and thus the transmitting receiver is completely removed. Since the results for different damage states are compared, it is important to have the same conditions of the experimental setup for every test. In Figure 5.4 the results of five measurements taken on an undamaged specimen are presented. The level of the values varies by up to 15%. However, the slopes of the linear fit for the different measurements are close to each other and vary by less than 9%. The variation in the amplitude can be explained by the coupling condition. Before a measurement is started the transducers are coupled to the wedges each time. Variations in the amount of oil couplant or in the clamping force lead to a slightly different amplitude of the signal due to the variation in the transmission coefficient between the transducers and the wedges. But since these conditions do not change during one set of measurements and do not influence the nonlinear property of the specimen the slope of the line is not influenced.

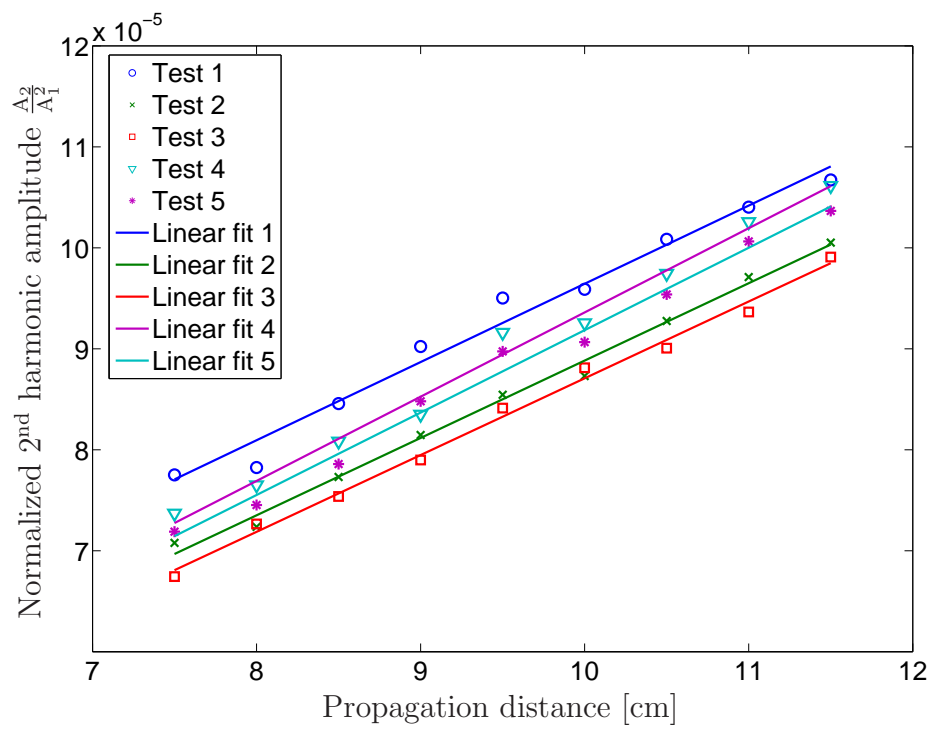


Figure 5.4: Multiple results of normalized second harmonic versus propagation distance.

5.3 Influence of Plastic Strain on Acoustic Nonlinearity

After taking baseline measurements of the nonlinearity of the material, one specimen is subjected to monotonic tension. The specimen is loaded up to a certain load level and then completely unloaded to allow for the ultrasonic measurement. After that, the specimen is loaded to the next load point. Figure 5.5 shows the stress-strain curves of the tests compared to the exploratory stress-strain relationship measured earlier. The specimen failed during the fifth test as marked in Figure 5.5. The disadvantage of using only one specimen and loading and unloading it repetitively is that the specimen undergoes a condition similar to a fatigue test with a very low number of cycles. The stress-strain curve indicates that strain hardening occurred. Using only one specimen however, has the advantage that the results measured at different load levels are directly comparable because local effects in the material and the surface roughness due to machining remain constant.

Figure 5.6 shows the results of the ultrasonic measurements. The plot shows the average value of the nonlinearity normalized by the baseline value over the total strain at the different load points. The error bars represent the standard deviation of three to four sets of measurements. The results show a clear increase in nonlinearity with increasing strain for the first three monotonic tests. The maximum value of the nonlinearity is about 30% above the initial value. The value of the nonlinearity drops at the fifth measurement. A possible reason for that is that although no apparent necking occurred until the fifth loading, the width of the specimen might still have decreased enough to cause a geometric influence on the propagating wave. Measurements for more specimens are needed to completely understand this drop.

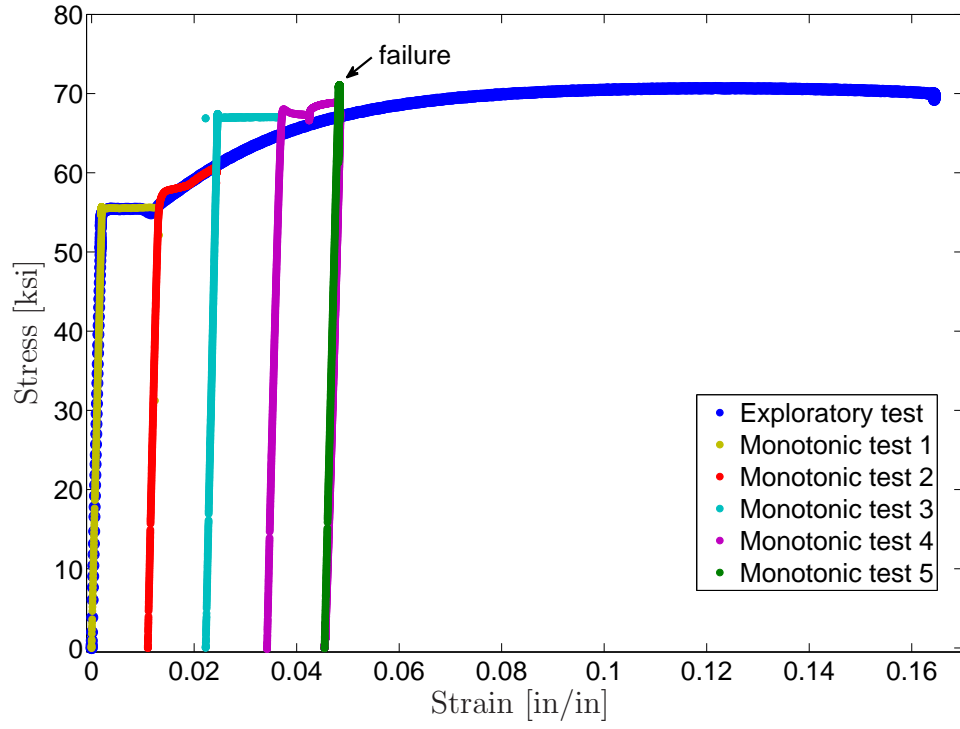


Figure 5.5: Stress-strain curves of the monotonic tests.

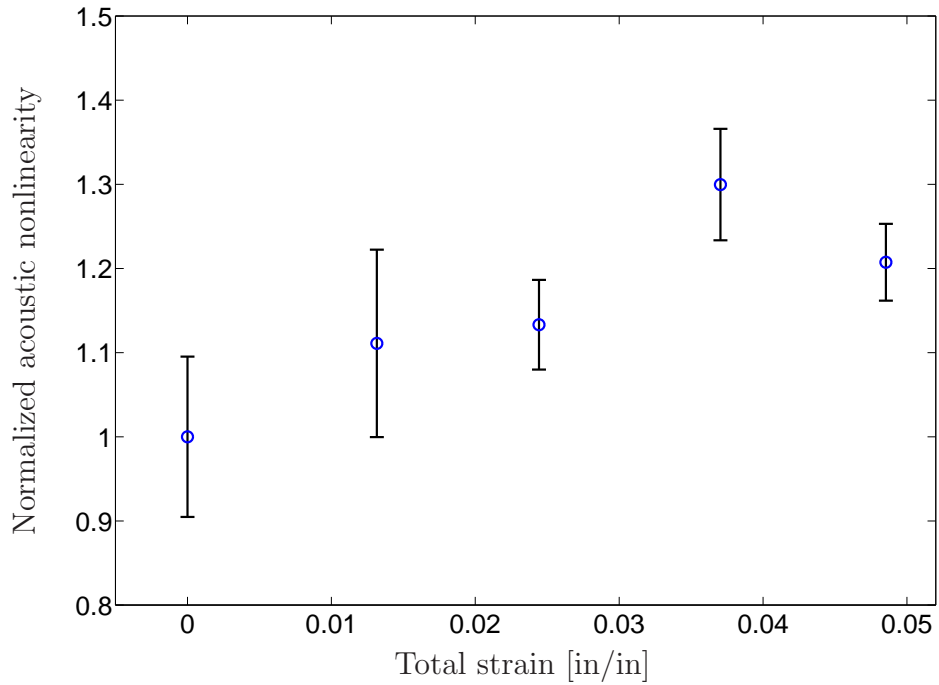


Figure 5.6: Normalized acoustic nonlinearity versus total strain.

5.4 *Influence of Fatigue Damage on Acoustic Nonlinearity*

In this section the influence of fatigue damage on the acoustic nonlinearity of A36 steel is characterized. The results for four specimens are presented separately. All specimens undergo a load-controlled tension-tension fatigue test with a stress ratio of 0.05 but with different maximum stresses.

5.4.1 Specimen 1

The first specimen undergoes a fatigue test with a constant maximum stress 10% above the yield stress determined from the result of the exploratory test. Therefore, a stress of 59.4 ksi is needed. The waveform of the fatigue cycles is a ramp function with a cycle rate of 0.5 Hz. The number of cycles applied in every fatigue test is shown in Table 5.1.

Figure 5.7 shows the stress in the specimen during the first three cycles of fatigue. It can be seen that the desired maximum stress level is not reached. The fatigue machine is not fully capable of following the designated load profile. For the following tests the nominal maximum and minimum loads are therefore adjusted so that the actual stresses in the material match the desired values.

The result of the ultrasonic measurements for increasing numbers of fatigue cycles is shown in Figure 5.8. The nonlinearity is normalized by the value of the baseline measurement on the undamaged specimen. The error bars are obtained by repeating the measurement three to five times. It should be noted that the first point does not correspond to one cycle of fatigue but represents the undamaged specimen. This is due to the fact that zero cycles cannot be displayed in this logarithmic plot.

Table 5.1: Number of fatigue cycles applied on specimen 1.

Cycles per test	3	5	10	20	50	100	300	500	1000	2000
Total cycle number	3	8	18	38	88	188	488	988	1988	3988

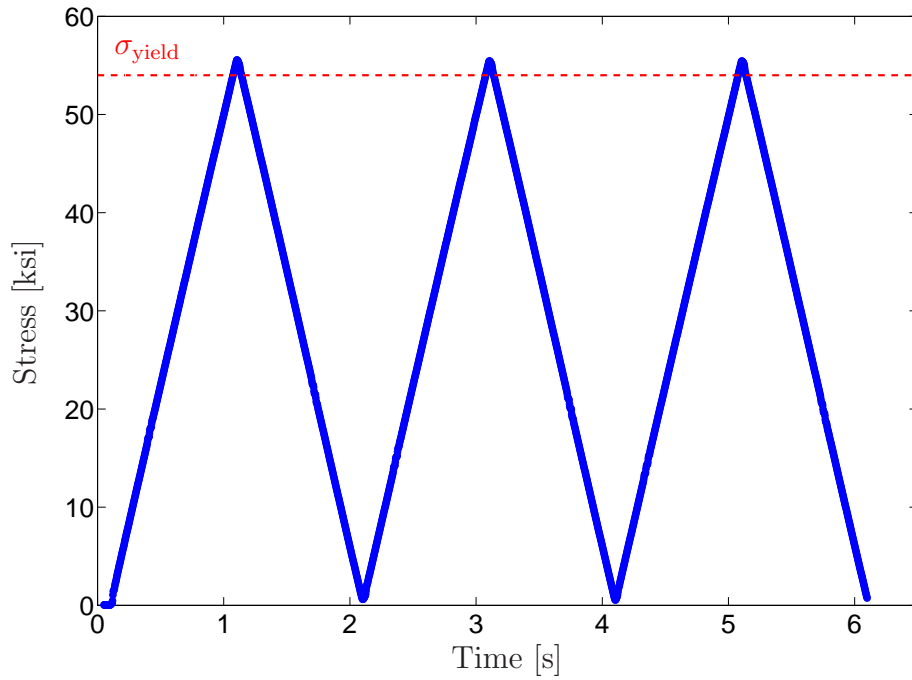


Figure 5.7: Stress versus time for the first fatigue test.

The plot shows some variation of the normalized nonlinearity. However, no clear trend is visible and most of the values are very close to the nonlinearity measured for the undamaged specimen. Besides the third point, which is not consistent with the other data, a small increase in nonlinearity can be observed for the very first numbers of cycles. But after 38 cycles the nonlinearity drops close to the baseline value. This decrease in nonlinearity can be explained by looking at the normalized second harmonic amplitude over the propagation distance. Figure 5.9a shows this relationship after the first fatigue test of three cycles. The expected linear relationship is obvious. On the other hand, Figure 5.9b shows the same plot after 38 cycles of fatigue. Here, the trend is not perfectly linear anymore; it rather looks like two shifted parallel lines. Because of the described behavior, taking the slope of the linear fit in the range of 7.5 cm to 11.5 cm for more than 38 cycles results in a relatively low value of the acoustic nonlinearity. The technique of varying the propagation distance of

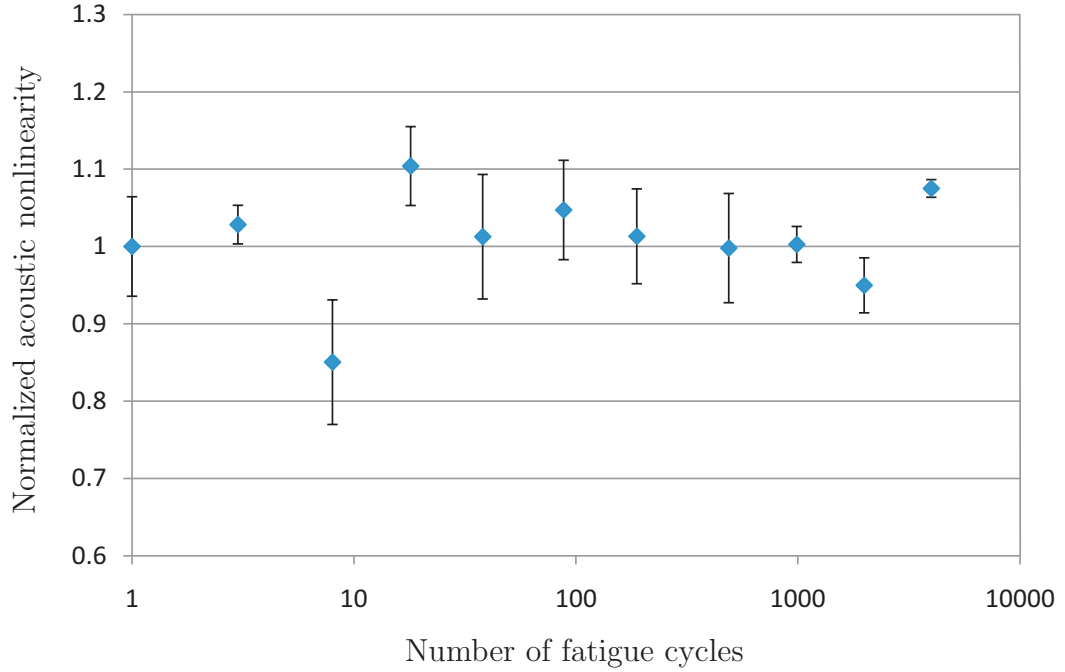
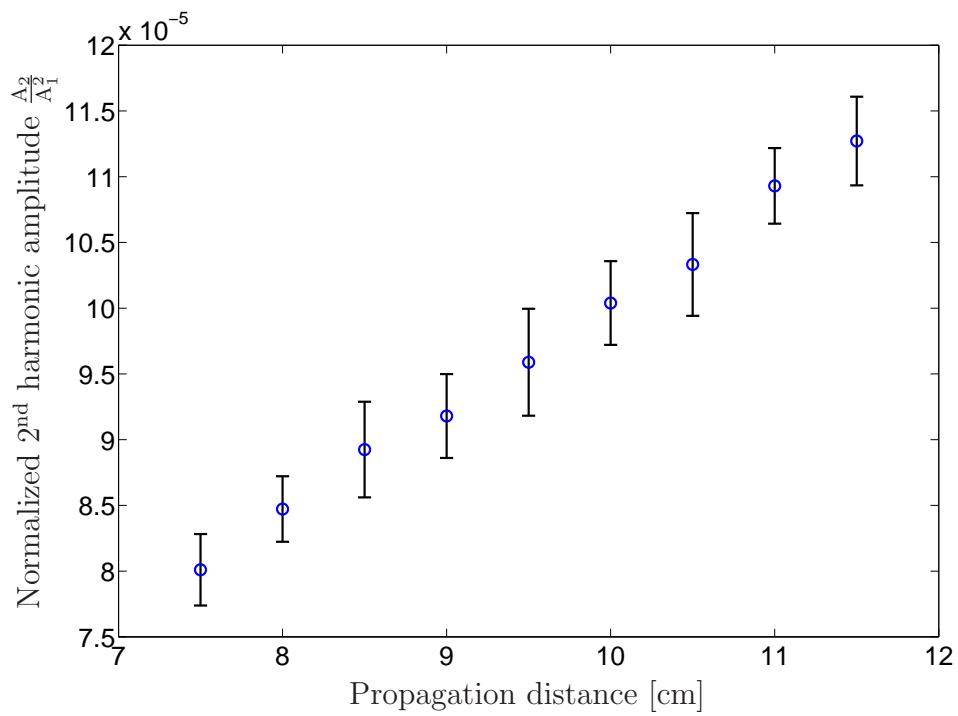


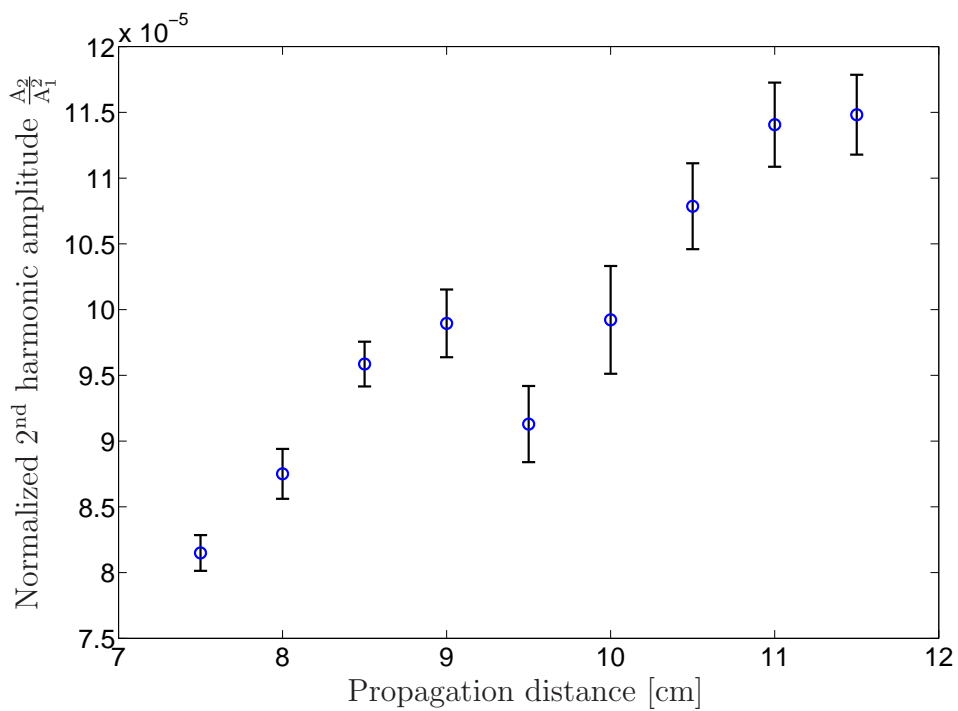
Figure 5.8: Normalized acoustic nonlinearity versus number of fatigue cycles for specimen 1 for $\sigma_{\max} = 1.1 \sigma_{\text{yield}}$, $R=0.05$ and a propagation distance from 7.5 cm to 11.5 cm.

the Rayleigh waves provides a value of the average nonlinearity over the scanned propagation distance. The influence of localized effects on the acoustic nonlinearity cannot be detected accurately. All measurements taken after 38 or more cycles show the behavior of a drop in the normalized second harmonic for a propagation of 9.5 cm. This indicates that some local effect in the material must be the reason.

Indeed, a surface damage on the specimen was found at a distance of 9.5 cm from the transmitting wedge. This corresponds to the distance at which the normalized second harmonic drops. Since the specimen was carefully surface ground before the first measurements were taken, the damage must have occurred after this mechanical testing started. Figure 5.10 shows a picture of a sections of the specimen. The circle marks a scratch with a length of approximately 4 mm. The orientation of the scratch is perpendicular to the propagation direction of the Rayleigh wave. As shown in Figure 5.11 the scratch has no noticeable influence on the amplitude of



(a) 3 cycles



(b) 38 cycles

Figure 5.9: Normalized second harmonic amplitude versus propagation distance for specimen 1 after different numbers of fatigue cycles.

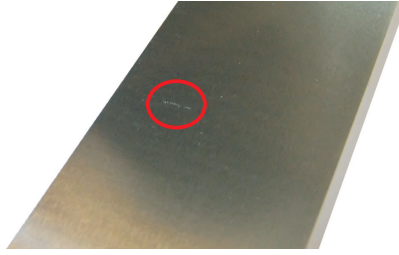


Figure 5.10: Image of surface damage on fatigue specimen 1.

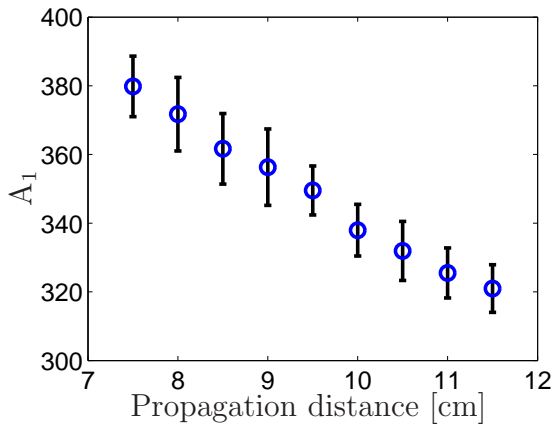


Figure 5.11: Amplitude of the fundamental over the propagation distance after 38 cycles.

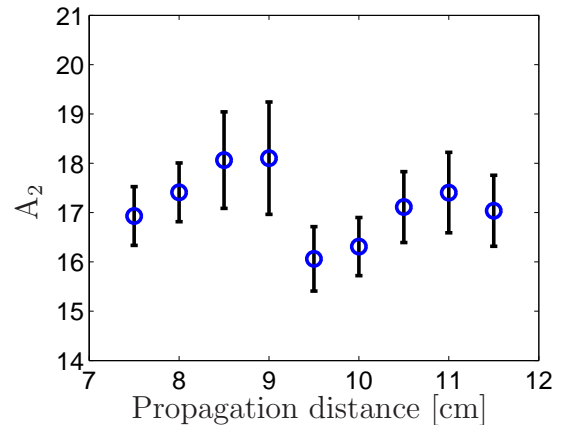


Figure 5.12: Amplitude of the second harmonic over the propagation distance after 38 cycles.

the fundamental frequency. However, Figure 5.12 shows that the second harmonic amplitude drops for a propagation distance of 9.5 cm. This can be explained by the fact that the wavelength of the second harmonic is shorter than the wavelength of the fundamental since $\lambda = c/f$. Therefore the penetration depth of the second harmonic is also lower. This makes the second harmonic amplitude much more sensitive to small surface scratches because a larger portion of the second harmonic is reflected at imperfections.

If only the data for a propagation distance between 7.5 cm and 8.5 cm is used the result shown in Figure 5.13 is obtained. In this plot the local behavior for a small section of the specimen is shown and the effect of the surface damage is excluded. But since only three data points are used the error bars are very large and thus the

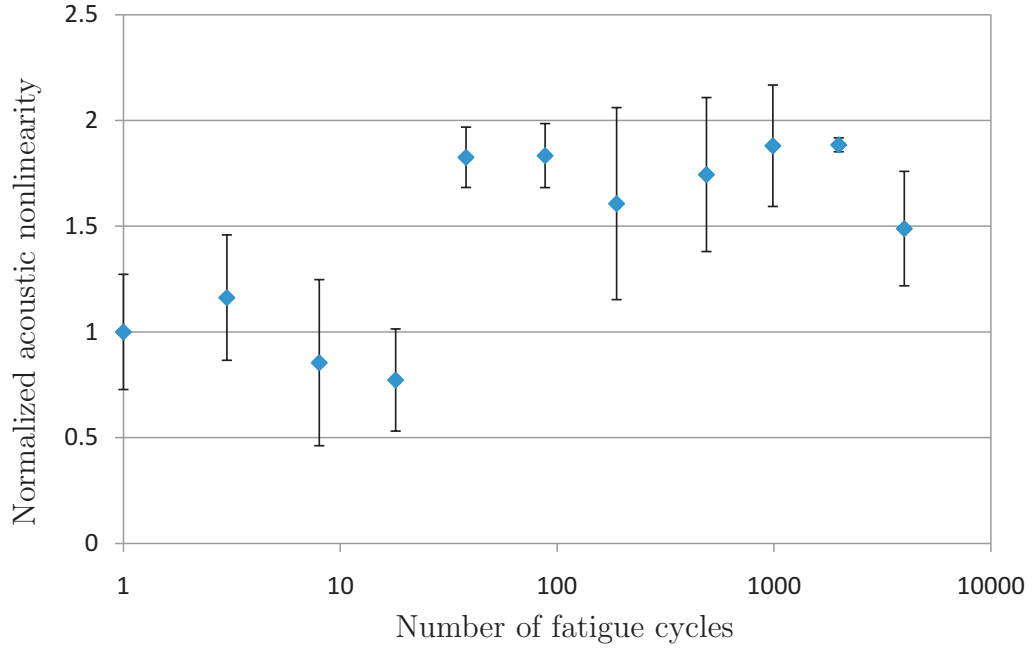


Figure 5.13: Normalized acoustic nonlinearity versus number of fatigue cycles for specimen 1 for a propagation distance from 7.5 cm to 8.5 cm.

values are less reliable. This result shows a large increase in acoustic nonlinearity after the fourth fatigue test. After that, the acoustic nonlinearity stays constant at a high level.

Measurements are also taken on the backside of the same specimen. The results of these measurements are shown in Figure 5.14. The propagation distance in this case is varied from 7.5 cm to 11.5 cm. No measurements are taken for low numbers of fatigue cycles. Note that on this side of the specimen the measurements are only repeated once or twice for each damage state. Therefore, the error bars are relatively large. The general trend of this plot shows that the nonlinearity of the damaged material is higher than for the undamaged one but for high numbers of cycles no large variation of the acoustic nonlinearity is observed.

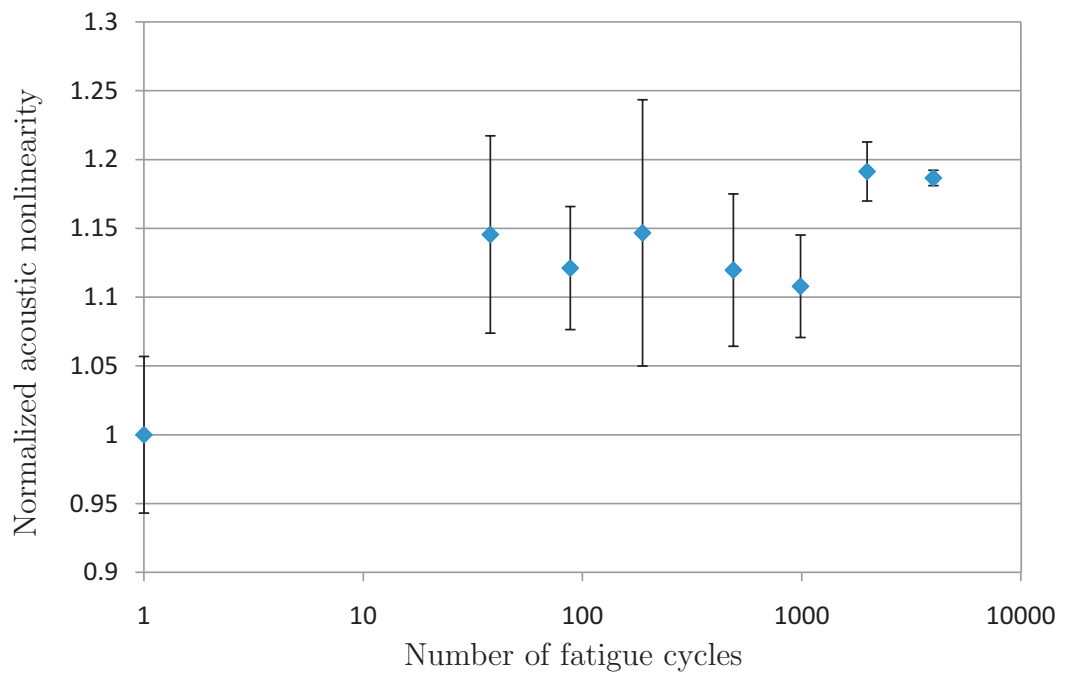


Figure 5.14: Normalized acoustic nonlinearity versus number of fatigue cycles for specimen 1 measured on the backside.

5.4.2 Specimen 2

The second specimen is subjected to a slightly higher load than the first specimen. The maximum stress for this specimen is 1.15 times the yield strength. Table 5.2 shows the number of fatigue cycles applied on this specimen during each fatigue test. Again, the waveform is a ramp function with a frequency of 0.5 Hz.

During the first three cycles little plastic deformation occurs in the area where the extensometer is attached to the specimen. One reason for this is that the fatigue machine needs some time to reach a stabilized stress level at the beginning of a fatigue test. During the next numbers of cycles however, plastic deformation is measured by the extensometer after unloading the specimen. Figure 5.15 shows the stress-strain curve of the third fatigue test on this specimen. In this test the specimen undergoes ten cycles of fatigue with a constant stress amplitude. Plastic deformation is clearly visible and the plot furthermore shows that the amount of plastic strain per cycle decreases with increasing number of fatigue cycles. This is due to strain-hardening in the specimen. For higher numbers of fatigue cycles very little plastic deformation occurs. In Figure 5.16 the hysteresis curves of fatigue test four are shown for the first, second, and last cycle. This corresponds to the total cycle numbers 19, 20, and 38.

Ultrasonic measurements are taken for varying propagation distances after every fatigue test. Figure 5.17 shows the results of these measurements for the undamaged specimen and after 88 cycles of fatigue as an example. The slope of the linear fit of the damaged specimen is found to be higher than the slope of the linear fit of the undamaged specimen and also the level of the values after 88 cycles is higher

Table 5.2: Number of fatigue cycles applied on specimen 2.

Cycles per test	3	5	10	20	50	100	300	1000	3000	5000	5000
Total cycle number	3	8	18	38	88	188	488	1488	4488	9488	14488

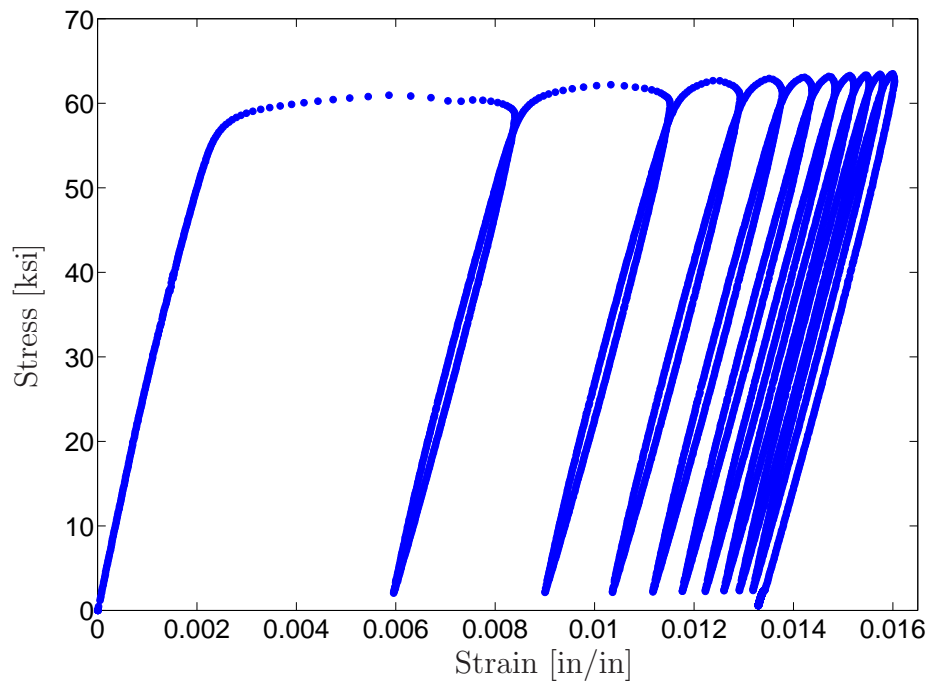


Figure 5.15: Stress-strain curve for fatigue test 3 on specimen 2.

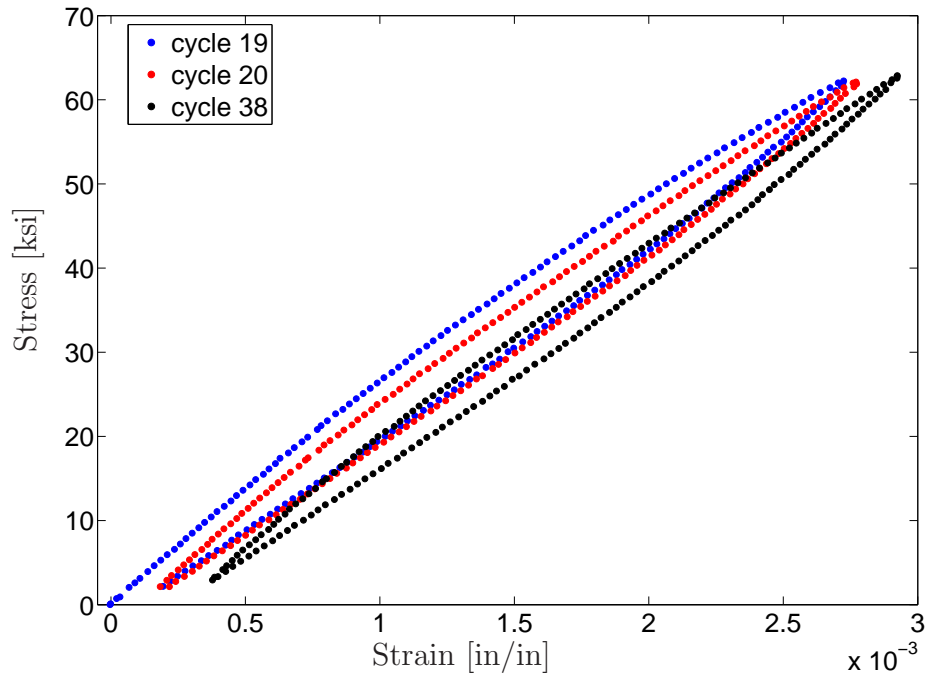


Figure 5.16: Stress-strain curve for fatigue test 4 on specimen 2.

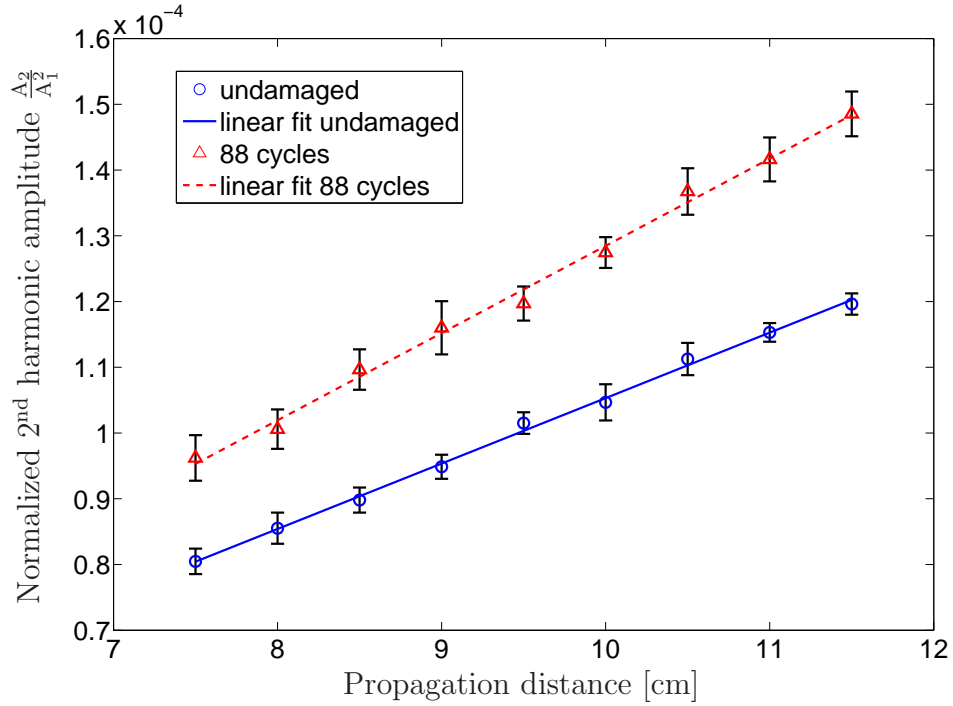


Figure 5.17: Normalized second harmonic amplitude versus propagation distance for the undamaged specimen and after 88 cycles of fatigue.

than for the undamaged case. Note that the trend of the data after 88 cycles is very linear. This behavior does not change significantly for higher numbers of cycles. This indicates that the fatigue damage is evenly distributed throughout the scanned section of the specimen. However, localized damage might have occurred outside the scanned section, since failure occurred outside this area.

An interesting behavior can also be observed if the results of the ultrasonic measurements after the first three fatigue tests are considered. Figure 5.18 shows the normalized second harmonic amplitude versus propagation distance for these three cases. It is seen that the trend after three cycles is linear. However, after eight cycles the values are scattered. This might be an indication for localized damage in the very early fatigue life. After the next fatigue test the trend goes back to a more linear relationship. Therefore, the damage is assumed to be more evenly distributed. As mentioned above, this linear trend remains for higher numbers of fatigue cycles.

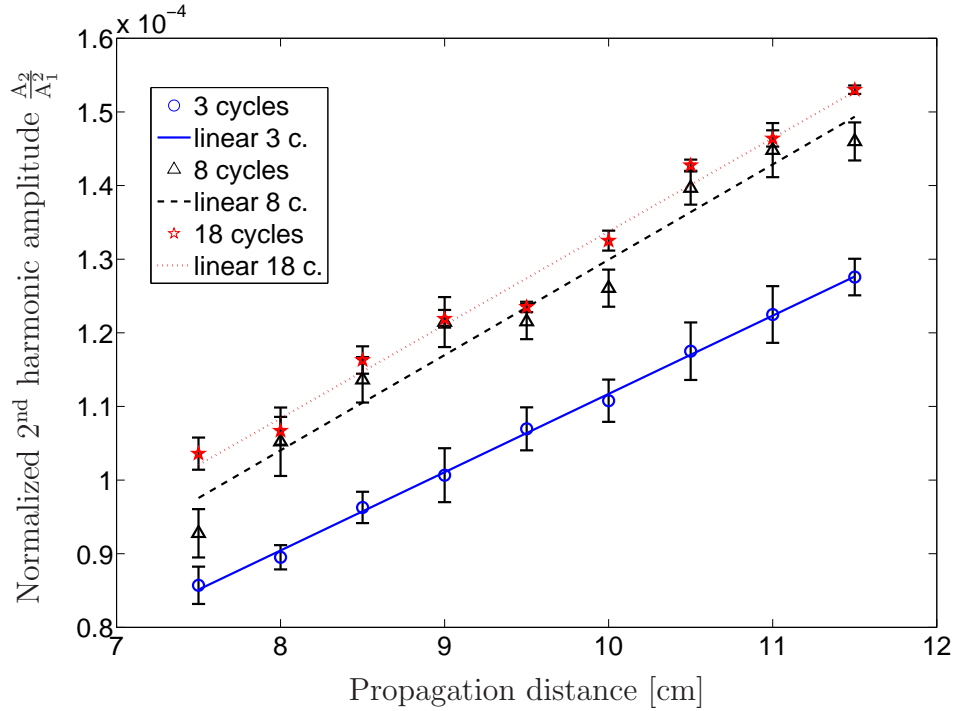


Figure 5.18: Normalized second harmonic amplitude versus propagation distance after the first three fatigue tests.

In Figure 5.19 the results of the ultrasonic measurements as well as the measured cumulative plastic strain are combined. Note that the first points correspond to the undamaged specimen again. The cumulative plastic strain shows a steep increase after the second and third fatigue test. After that, the plastic strain stays almost constant. Only for very high numbers of cycles the strain increases again.

The acoustic nonlinearity is normalized by the value of the undamaged specimen and the error bars result from repeated ultrasonic measurements on the same specimen. The acoustic nonlinearity shows a large increase after a small number of cycles. The value for eight cycles is significantly high and the error bar is large. This can be explained by the nonlinear behavior of the normalized second harmonic versus the propagation distance as described above. After more than 100 cycles the nonlinearity saturates. The level of saturation is 30% above the initial acoustic nonlinearity of the undamaged specimen. Noticeable is the correlation between the characteristics of

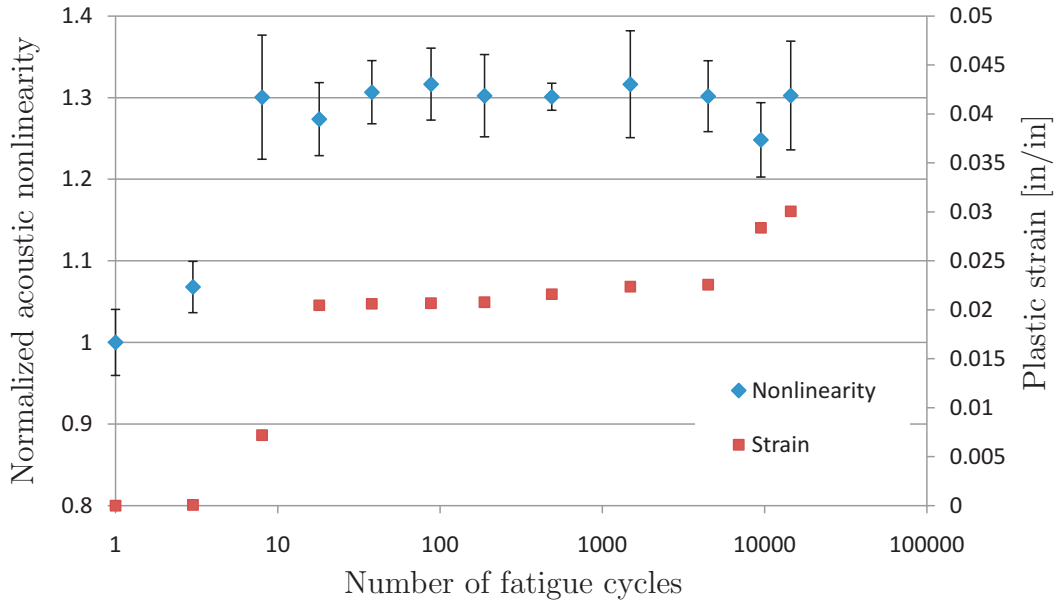


Figure 5.19: Normalized acoustic nonlinearity and cumulative plastic strain versus number of fatigue cycles for specimen 2 for $\sigma_{\max} = 1.15 \sigma_{\text{yield}}$, $R=0.05$, and a propagation distance from 7.5 cm to 11.5 cm.

the cumulative plastic strain and the acoustic nonlinearity. The acoustic nonlinearity follows the trend of the cumulative plastic strain very closely.

If the measured data is evaluated for a smaller range of the propagation distance Figure 5.20 is obtained. Here the slope of the linear fit for a propagation distance between 8.5 cm and 10.5 cm is used to get the normalized acoustic nonlinearity. For this range the acoustic nonlinearity follows the trend of the cumulative plastic strain even closer. This result indicates that the acoustic nonlinearity in A36 steel is highly plasticity driven. The advantage of using a smaller range of the propagation distance is that the local damage state is detected. However, since less data points are used the accuracy is lower and the error bars are larger. Furthermore, in field applications the damage state of entire, large structures is of interest. Therefore a large range of the propagation distance is needed. For this purpose, some inversion procedure to calculate the nonlinearity parameter as a function of propagation distance is needed.

The step increase in early fatigue life corresponds well to the observations of

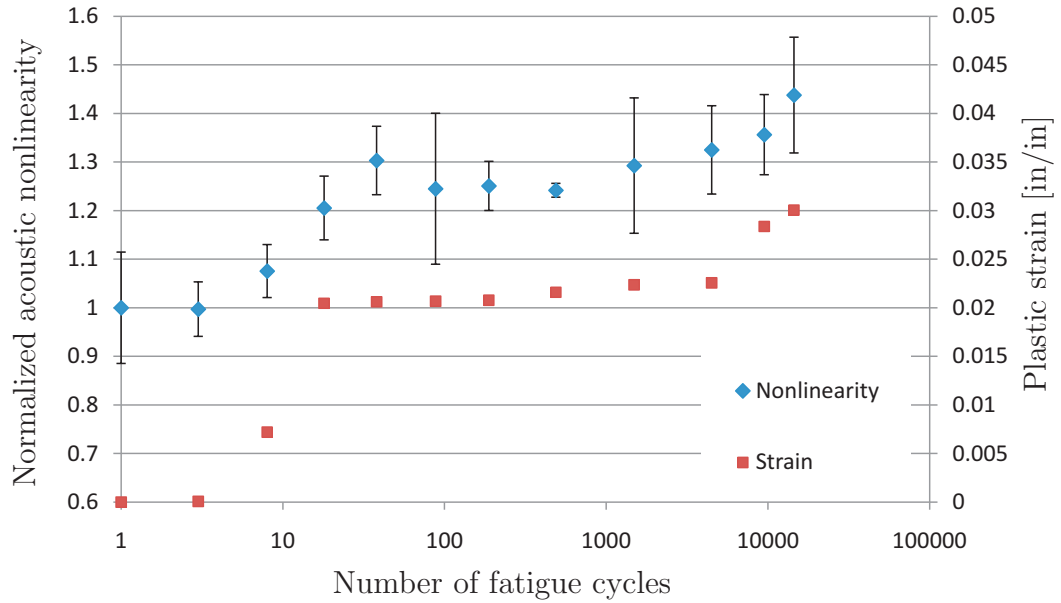


Figure 5.20: Normalized acoustic nonlinearity and cumulative plastic strain versus number of fatigue cycles for specimen 2 for $\sigma_{\max} = 1.1 \sigma_{\text{yield}}$, $R=0.05$ and a propagation distance from 8.5 cm to 10.5 cm.

Amaro [2] for a different material. Amaro showed that the slip band spacing in a single crystal superalloy decreases rapidly only over the first few fatigue cycles which means that the slip system activation is localized in the material within the first few cycles of inelastic deformation. Since the Rayleigh wave is sensitive to the creation of persistent slip bands the increase of the acoustic nonlinearity in the early fatigue life is comprehensible. During further cycling the slip band spacing and therefore, the number of slip bands saturates leading to little variation in the acoustic nonlinearity.

5.4.3 Specimen 3

After getting the results for the relatively high maximum load for specimen 2, specimen 3 is subjected to a lower load. The maximum stress for this specimen is chosen close to the yield stress. In addition, the cycle rate is increased to 1 Hz. The number of cycles for this specimen can be found in Table 5.3.

Figure 5.21 shows the normalized acoustic nonlinearity and the cumulative plastic strain over the number of cycles. For this specimen no large change in the acoustic nonlinearity is recorded. After the first cycles the acoustic nonlinearity is decreasing. However, the decrease is smaller than 10%. After the fourth fatigue test a small increase in the acoustic nonlinearity is visible that correlates with the increase in plastic strain measured by the extensometer. But more cycles of fatigue do not lead to a further increase either in the acoustic nonlinearity or in the plastic strain.

The cumulative plastic strain shown in Figure 5.21 only shows an increase after the fourth fatigue test. This can be explained by the formation of Lüders lines. The maximum stress used for this specimen is approximately the yield stress of the material. During the fourth fatigue test Lüders lines visible with the naked eye appeared on the surface of the specimen and propagated along the loading axis. These marks are caused by localized inhomogeneous yielding.

The fact that the damage is very localized in the material could be an explanation for the behavior of the acoustic nonlinearity shown in Figure 5.21. Since the acoustic nonlinearity is determined by varying the propagation distance between transmitter and receiver the effects of localized damage may be averaged out. Therefore no large variations in the acoustic nonlinearity are measured.

Table 5.3: Number of fatigue cycles applied on specimen 3.

Cycles per test	3	7	20	100	500	1370
Total cycle number	3	10	30	130	630	2000

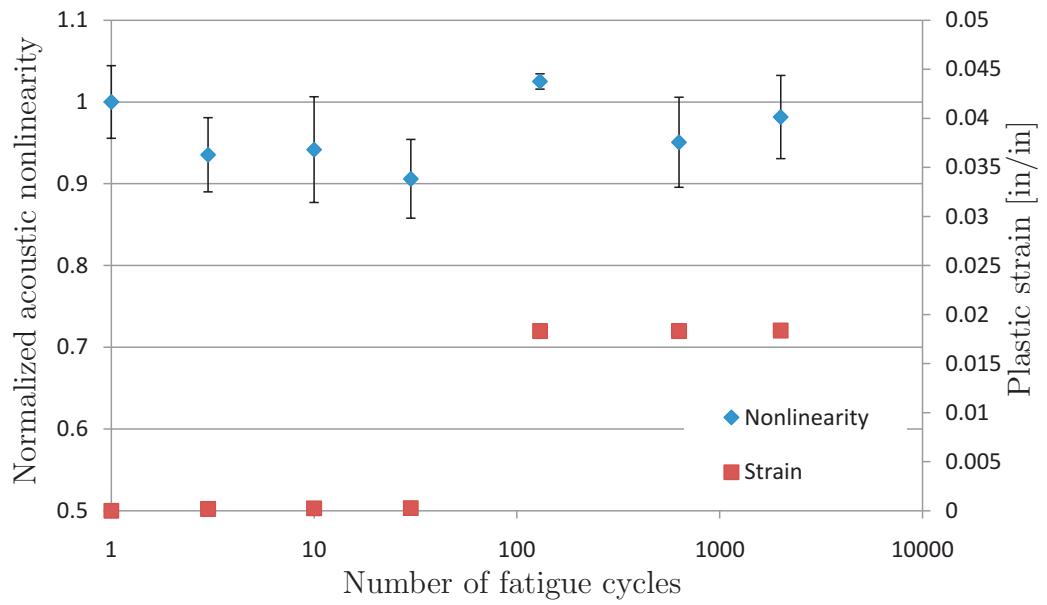


Figure 5.21: Normalized acoustic nonlinearity and cumulative plastic strain versus number of fatigue cycles for specimen 3 for $\sigma_{\max} = 1.06 \sigma_{\text{yield}}$, $R=0.05$ and a propagation distance from 7.5 cm to 11.5 cm.

5.4.4 Specimen 4

For the last specimen a higher maximum stress is used again. Here, the maximum stress is 16% above the yield stress. For high numbers of cycles the maximum stress increased slightly to 19% above the yield stress due to inconsistency in the load applied by the fatigue machine. Table 5.4 summarizes the numbers of fatigue cycles used for specimen 4.

In Figure 5.22 the results of the ultrasonic measurements and the cumulative plastic strain are shown. As before, the first point corresponds to the undamaged specimen and the depicted strain is the strain measured by the extensometer in the area where the receiving transducer is scanned. For the ultrasonic measurements, the propagation distance is varied between 7.5 cm and 11.5 cm. The cumulative strain in this area shows a large increase during the second fatigue test and little variation for higher numbers of cycles. The measured acoustic nonlinearity does not change during the very first fatigue test but shows an increase for the next two tests. Then, the value of the acoustic nonlinearity stays constant until for very high numbers of cycles when a decrease is visible. Especially for less than 1000 cycles the behavior of the acoustic nonlinearity corresponds well with the trend of the cumulative plastic strain. A similar observation was made for specimen 2 in Section 5.4.2. This supports the assumption of the plasticity driven behavior of the acoustic nonlinearity in this material.

Recall that the acoustic nonlinearity shown in Figure 5.22 is based on the average value for the area over which the receiving wedge is scanned. For specimen 2 it was shown that the damage in the scanned section was evenly distributed, the

Table 5.4: Number of fatigue cycles applied on specimen 4.

Cycles per test	3	5	10	20	50	312	1600	6000
Total cycle number	3	8	18	38	88	400	2000	8000

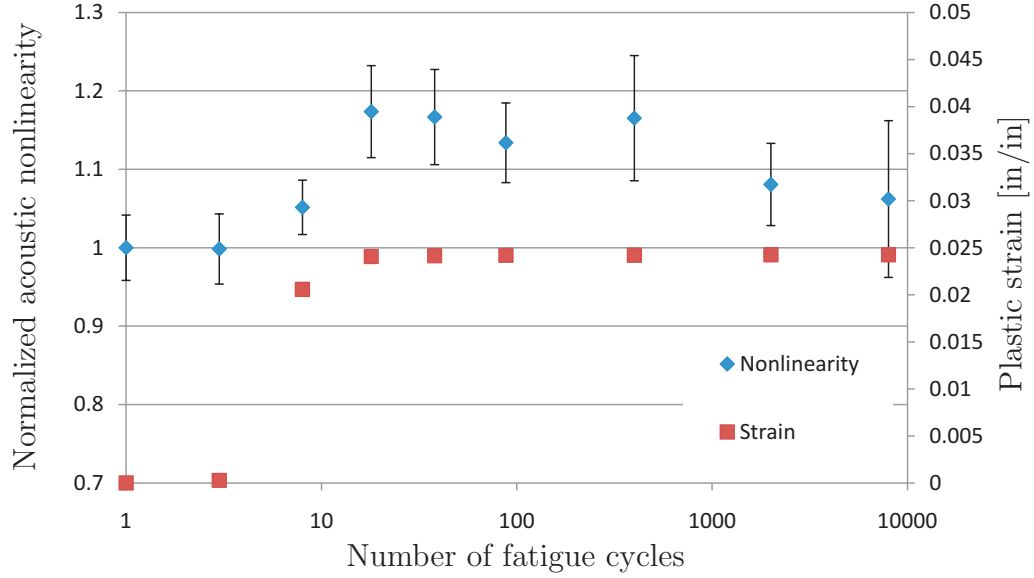
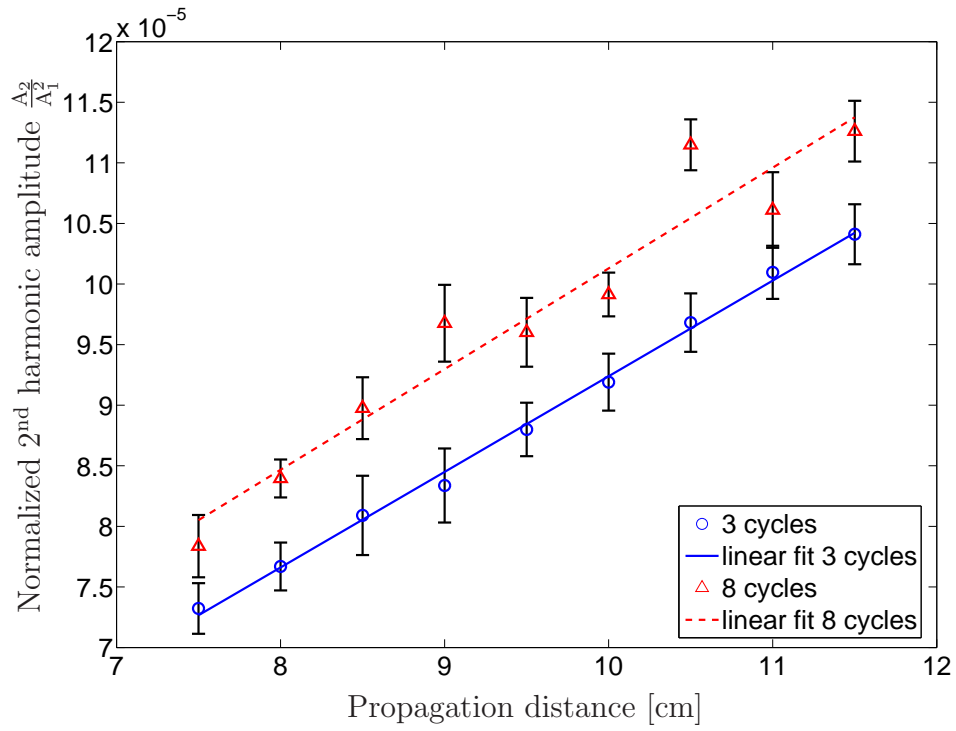
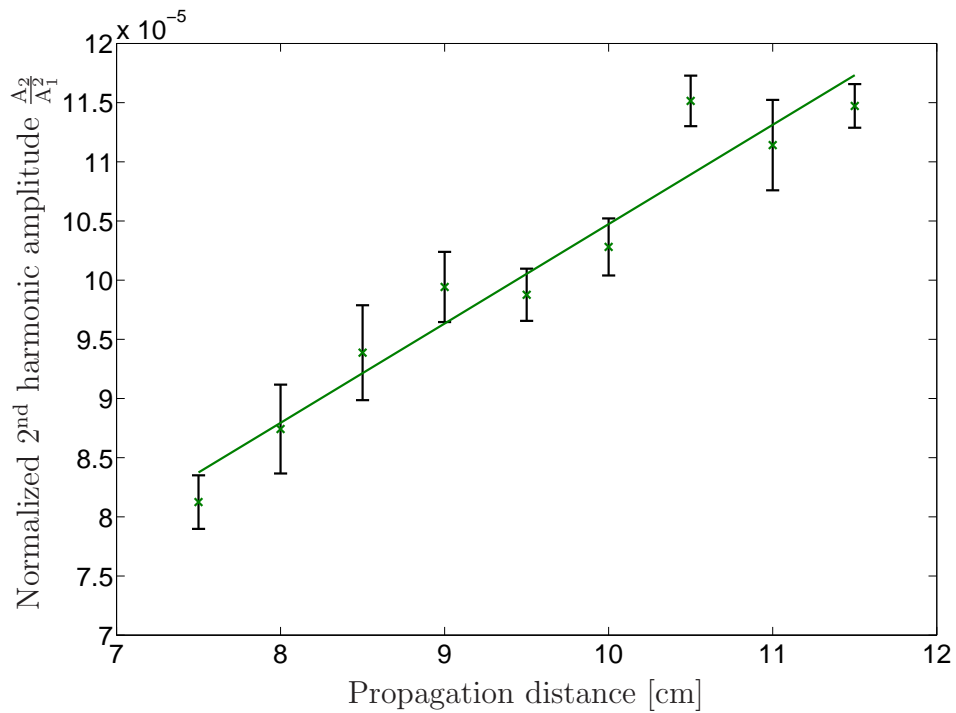


Figure 5.22: Normalized acoustic nonlinearity and cumulative plastic strain versus number of fatigue cycles for specimen 4 for $\sigma_{\max} = 1.16 \sigma_{\text{yield}}$, $R=0.05$ and a propagation distance from 7.5 cm to 11.5 cm.

trend of $\frac{A_2}{A_1^2}$ versus the propagation distance is very linear. However, this is not the case for specimen 4. In Figure 5.23 the normalized second harmonic amplitude versus the propagation distance for different damage states is shown. After the first 3 cycles of fatigue the trend is linear. But after the next fatigue test the values are scattered more. For example the value for a propagation distance of 9.5 cm is relatively low whereas the value for 10.5 cm is relatively high. This trend remains the same for higher number of cycles, the plot for 8000 cycles is shown in Figure 5.23b. The acoustic nonlinearity is therefore not constant throughout the material. This behavior indicates that the fatigue damage is not evenly distributed. As described earlier, fatigue damage in steel initiates in the form of slip bands in grains having an unfavorable orientation to the applied stress. As the saturation level is approached, few additional slip bands are formed but the localized, present slip bands become more emphasized. Using the slope of the linear fit results in the acoustic nonlinearity, averaged over the propagation distance. Therefore, the local damage is not clearly



(a) 3 and 8 cycles



(b) 8000 cycles

Figure 5.23: Normalized second harmonic amplitude versus propagation distance for specimen 4 after different numbers of fatigue cycles.

detected.

Looking at the data of the normalized second harmonic amplitude versus the propagation distance gives rise to the need to solve inverse problem of how the damage is distributed throughout the material. The curves for more than eight cycles in Figure 5.23 show a linear trend for the first four points. For a propagation distance of 9.5 cm and 10 cm the value is lower and for 10.5 cm a large increase is visible. This may be an indication of localized damage. For an exact analysis of the damage distribution however, the stepsize of the scanning along the loading axis should be reduced. This is difficult to achieve and very time consuming if the wedge method is used. For this specific task a non-contact method would be much more efficient.

CHAPTER VI

CONCLUSION

In this research, Rayleigh surface waves are used to characterize damage due to static loading and fatigue in A36 steel specimens. A reliable and efficient measurement technique is developed and changes in the acoustic nonlinearity are observed.

The ultrasonic measurements are successfully performed using the wedge method for generation and detection of the Rayleigh surface waves. Fluid coupling is used between the transducers and the wedges as well as between the wedges and the specimen. The high power input signal needed for the generation of the second harmonic is produced by a gated high power amplifier with high system linearity. The developed method is robust and allows repeatable measurements. However, the clamping of the wedge to the specimen needs to be improved to further enhance the accuracy.

After a Hann window is applied on the received signal, a fast Fourier transform is performed in order to get the amplitudes of the fundamental and second harmonic component. Ultrasonic measurements are performed for various propagation distances of the Rayleigh surface wave. The normalized second harmonic amplitude A_2/A_1^2 is found to increase linearly with an increasing propagation distance as expected.

The dogbone shaped specimens made of A36 steel are subjected to monotonic tensile and tension-tension fatigue load and the relative acoustic nonlinearity is compared for different damage states. It is shown that the acoustic nonlinearity increases with plastic strain for A36 steel during a monotonic tension test. The maximum value of the acoustic nonlinearity is 30% above the initial value of the undamaged specimen.

Since Rayleigh waves propagate along the free surface, the surface conditions and

the surface roughness are critical. Surface damage leads to a nonlinear relationship between the normalized second harmonic and the propagation distance. Due to the high sensitivity of the second harmonic the position of a surface scratch is found on one specimen. However, this behavior hinders the accurate detection of the acoustic nonlinearity.

Even if no surface damage is present, the normalized second harmonic amplitude versus the propagation distance does not always show a completely linear trend. This is due to the fact that the fatigue damage is not evenly distributed throughout the material. In this work the nonlinearity averaged over a certain propagation distance is evaluated. If the area is small only a few data points can be used which results in less reliable results. Localized damage leads to variations in the amplitude of the second harmonic. Therefore, the inverse problem can be posed which is on how the damage is distributed. However, the area should be scanned using a small stepsize. Therefore it would be convenient to use a non-contact method such as the laser interferometry.

For the fatigued specimens, a dependance of the acoustic nonlinearity on the number of fatigue cycles is observed. For two specimens a large increase of 20 % and 30 % in acoustic nonlinearity over the early fatigue life is shown. For higher numbers of cycles the changes in acoustic nonlinearity are less significant. This can be a key input to the remaining lifetime prediction strategy based on the fatigue-fracture framework. Furthermore, the acoustic nonlinearity shows a very close correlation with the cumulative plastic strain. This indicates that the acoustic nonlinearity for A36 steel is highly plasticity driven. This observation could be used to develop an alternative nondestructive technique to measure the cumulative plastic strain in a structure made of A36 steel.

REFERENCES

- [1] ACHENBACH, J., *Wave propagation in elastic solids*. North-Holland series in applied mathematics and mechanics, North-Holland, 1999.
- [2] AMARO, R. L., *Thermomechanical fatigue crack formation in a single crystal Ni-base superalloy*. PhD thesis, Georgia Institute of Technology, 2011.
- [3] BARNARD, D. J., BRASCHE, L. J. H., RAULERSON, D., and DEGTYAR, A. D., “Monitoring fatigue damage accumulation with Rayleigh wave harmonic generation measurements,” *Review of Progress In Quantitative Nondestructive Evaluation*, vol. 22, pp. 1393–1400, 2003.
- [4] BLACKSHIRE, J. L., SATHISH, S., NA, J., and FROUIN, J., “Nonlinear laser ultrasonic measurements of localized fatigue damage,” *Review of Progress In Quantitative Nondestructive Evaluation*, vol. 22, pp. 1479–1488, 2003.
- [5] CANTRELL, J. H., “Substructural organization, dislocation plasticity and harmonic generation in cyclically stressed wavy slip metals,” *Proceedings of the Royal Society of London Series A-mathematical Physical and Engineering Sciences*, vol. 460, pp. 757–780, Mar. 2004.
- [6] CANTRELL, J. H. and YOST, W. T., “Nonlinear ultrasonic characterization of fatigue microstructures,” *International Journal of Fatigue*, vol. 23, pp. S487–S490, 2001.
- [7] CANTRELL, J. H., “Ultrasonic harmonic generation from fatigue-induced dislocation substructures in planar slip metals and assessment of remaining fatigue life,” *Journal of Applied Physics*, vol. 106, p. 093516, Nov. 2009.
- [8] DOWLING, N. E., *Mechanical behavior of materials: engineering methods for deformation, fracture, and fatigue*. McGraw-Hill series in materials science and engineering, Prentice Hall, 1999.
- [9] GRAFF, K., *Wave motion in elastic solids*. Dover books on engineering, Dover Publications, 1975.
- [10] GREEN, R., *Ultrasonic investigation of mechanical properties*. Treatise on materials science and technology, Academic Press, 1973.
- [11] HAMILTON, M. and BLACKSTOCK, D., *Nonlinear acoustics*. Academic Press, 1998.
- [12] HAO, S., “I-35w bridge collapse,” *Journal of Bridge Engineering*, vol. 15, pp. 608–614, Sept. 2010.

- [13] HERRMANN, J., JACOBS, L. J., QU, J. M., and KIM, J.-Y., “Generation and detection of higher harmonics in Rayleigh waves using laser ultrasound,” *Review of Progress in Quantitative Nondestructive Evaluation*, vol. 25, pp. 262–269, 2006.
- [14] HERRMANN, J., KIM, J.-Y., JACOBS, L. J., QU, J. M., LITTLES, J. W., and SAVAGE, M. F., “Assessment of material damage in a nickel-base superalloy using nonlinear Rayleigh surface waves,” *Journal of Applied Physics*, vol. 99, no. 12, 2006.
- [15] JIN, F., WANG, Z., and KISHIMOTO, K., “Basic properties of rayleigh surface wave propagation along curved surfaces,” *International Journal of Engineering Science*, vol. 43, no. 3-4, pp. 250 – 261, 2005.
- [16] KIM, J.-Y., QU, J., JACOBS, L. J., LITTLES, J. W., and SAVAGE, M. F., “Acoustic nonlinearity parameter due to microplasticity,” *Journal of Nondestructive Evaluation*, vol. 25, pp. 29–37, Mar. 2006.
- [17] LARSON, G. D., MARTIN, J. S., and SCOTT JR., W. R., “Seismic landmine detection using microphones as near-ground sensors.,” *Journal of the Acoustical Society of America*, vol. 117, pp. 2385–2385, Apr. 2005.
- [18] LIU, M., KIM, J.-Y., JACOBS, L., and QU, J., “Experimental study of non-linear Rayleigh wave propagation in shot-peened aluminum plates-feasibility of measuring residual stress,” *Ndt & E International*, vol. 44, pp. 67–74, Jan. 2010.
- [19] MUGHRABI, H., “Cyclic hardening and saturation behavior of copper single-crystals,” *Materials Science and Engineering*, vol. 33, no. 2, pp. 207–223, 1978.
- [20] OPPENHEIM, A., SCHAFER, R., and BUCK, J., *Discrete-time signal processing*. Prentice-Hall signal processing series, Prentice Hall, 1999.
- [21] PRUELL, C., KIM, J.-Y., QU, J. M., and JACOBS, L. J., “Evaluation of fatigue damage using nonlinear guided waves,” *Smart Materials & Structures*, vol. 18, p. 035003, Mar. 2009.
- [22] SAGAR, S. P., METYA, A. K., GHOSH, M., and SIVAPRASAD, S., “Effect of microstructure on non-linear behavior of ultrasound during low cycle fatigue of pearlitic steels,” *Materials Science and Engineering A-structural Materials Properties Microstructure and Processing*, vol. 528, pp. 2895–2898, Mar. 2011.
- [23] SHUI, Y. G. and SOLODOV, I. Y., “Nonlinear properties of Rayleigh and Stoneley waves in solids,” *Journal of Applied Physics*, vol. 64, pp. 6155–6165, Dec. 1988.
- [24] SURESH, S., *Fatigue of materials*. Cambridge solid state science series, Cambridge University Press, 1998.

- [25] VALLURI, J. S., BALASUBRAMANIAM, K., and PRAKASH, R. V., “Creep damage characterization using non-linear ultrasonic techniques,” *Acta Materialia*, vol. 58, pp. 2079–2090, Apr. 2010.
- [26] VIKTOROV, I., *Rayleigh and Lamb Waves, Physical Theory and Applications*. Plenum Press New York, 1967.
- [27] ZABOLOTSKAYA, E. A., “Nonlinear propagation of plane and circular Rayleigh waves in isotropic solids,” *The Journal of the Acoustical Society of America*, vol. 91, no. 5, pp. 2569–2575, 1992.